

Colour Deconfinement and Quarkonium Binding

Helmut Satz

Fakultät für Physik, Universität Bielefeld
Postfach 100 131, D-33501 Bielefeld, Germany

and

Centro de Física das Interações Fundamentais (CFIF)
Instituto Superior Técnico, Av. Rovisco Pais, P-1049-001 Lisboa, Portugal

Abstract:

At high temperatures, strongly interacting matter becomes a plasma of deconfined quarks and gluons. In statistical QCD, deconfinement and the properties of the resulting quark-gluon plasma can be investigated by studying the in-medium behaviour of heavy quark bound states. In high energy nuclear interactions, quarkonia probe different aspects of the medium formed in the collision. We survey the results of recent charmonium production studies in SPS and RHIC experiments.

Contents:

1. Introduction
2. Colour Deconfinement
3. Quarkonium Binding and Dissociation
4. Thermal Quarkonium Dissociation
5. Quarkonium Production in Nuclear Collisions
6. Experimental Results from Nucleus-Nucleus Collisions
7. Outlook

1. Introduction

The states of matter, their defining features and the transitions between them have always been among the most challenging problems of physics. Strongly interacting matter opens a new chapter for such studies. The elementary particles of strong interaction physics, the hadrons, make up most of the observable matter in the universe. They have intrinsic sizes and masses, and the ultimate aim of the theory of strong interactions is to derive these. Quantum chromodynamics (QCD) does that, in terms of massless gluons and almost massless quarks – it is their *dynamics* which generates the scales. Thus the nucleon is a bound state of three very light quarks; the kinetic and potential energy of the system provide the nucleon mass, and the binding potential determines the nucleon radius.

The interaction between quarks is based on their intrinsic colour charge, just as that between electrons and protons or nuclei is determined by their electric charge. The form of the interaction is quite different, however. The Coulomb potential vanishes for large separation distance, so that electric charges can be separated and have an independent existence. In contrast, the potential between quarks increases with separation, so that an infinite energy would be needed to isolate a quark. In other words, the quark constituents of a hadron are *confined* and not just bound.

Strong interaction *thermodynamics* shows that quark confinement has its inherent limits. As bound states of quarks, hadrons have an intrinsic size, the binding radius. At extreme density, when several hadrons are compressed into a spatial volume normally occupied by a single hadron, it becomes impossible to identify among all the overlapping states a specific quark-antiquark pair or quark triplet as belonging to a certain hadron. The medium becomes instead a dense multi-quark environment in which any quark can move as far as it wants, since it is always close enough to other quarks to satisfy confinement conditions. Confinement as a large distance feature thus loses its meaning in the short distance world of matter at extreme density.

It is therefore expected that with increasing temperature, strongly interacting matter will undergo a transition from a hadronic phase, in which the constituents are colour-neutral bound states, to a plasma of deconfined colour-charged quarks and gluons. This deconfinement transition in QCD is quite similar to the insulator-conductor transition in normal condensed matter physics: it corresponds to the onset of colour conductivity.

The thermodynamics of strongly interacting matter can be derived through first principle calculations in *finite temperature lattice QCD*, and we shall return to these studies in the next section. They provide quite detailed information on the temperature dependence of thermodynamic observables, such as pressure or energy density, and they show how these quantities change as the system passes through the deconfinement transition. This raises a crucial question: if we were given a box containing strongly interacting matter, how could we determine the temperature of the medium and how could we specify the state in which this medium is in? This question is the central topic of our survey, and we will show that the in-medium behaviour of *heavy quark* bound states provides an excellent tool to answer it.

Since some thirty years it is known that besides the almost massless *up* and *down* quarks of the everyday world, and the still relatively light *strange* quarks required to account for

the strange mesons and hyperons observed in hadron collisions, there are heavy quarks at the other end of the scale, whose bare masses alone are larger than those of most of the normal hadrons. These heavy quarks first showed up in the discovery of the J/ψ meson [1], of mass of 3.1 GeV; it is a bound state of a *charm* quark (c) and its antiquark (\bar{c}), each having a mass of some 1.2–1.5 GeV. On the next level there is the Υ meson [2], with a mass of about 9.5 GeV, made up of a *bottom* or *beauty* quark-antiquark pair ($b\bar{b}$), with each quark here having a mass around 4.5 - 4.8 GeV. Both charm and bottom quarks can of course also bind with normal light quarks, giving rise to open charm (D) and open beauty (B) mesons. The lightest of these ‘light-heavy’ mesons have masses of about 1.9 GeV and 5.3 GeV, respectively.

The bound states of a heavy quark Q and its antiquark \bar{Q} are generally referred to as quarkonia. Besides the initially discovered vector ground states J/ψ and Υ , both the $c\bar{c}$ and the $b\bar{b}$ systems give rise to a number of other *stable* bound states of different quantum numbers. They are stable in the sense that their mass is less than that of two light-heavy mesons, so that strong decays are forbidden. The measured stable charmonium spectrum contains the $1S$ scalar η_c and vector J/ψ , three $1P$ states χ_c (scalar, vector and tensor), and the $2S$ vector state ψ' , whose mass is just below the open charm threshold. There are further charmonium states above the ψ' ; these can decay into $D\bar{D}$ pairs, and we shall here restrict our considerations only to quarkonia stable under strong interactions. The observed stable charmonium states are summarized in table 1 and the corresponding bottomonium ($b\bar{b}$) states in table 2. The binding energies ΔE listed there are the differences between the quarkonium masses and the open charm or beauty threshold, respectively.

state	η_c	J/ψ	χ_{c0}	χ_{c1}	χ_{c2}	ψ'
mass [GeV]	2.98	3.10	3.42	3.51	3.56	3.69
ΔE [GeV]	0.75	0.64	0.32	0.22	0.18	0.05

Table 1: Charmonium states and binding energies

state	Υ	χ_{b0}	χ_{b1}	χ_{b2}	Υ'	χ'_{b0}	χ'_{b1}	χ'_{b2}	Υ''
mass [GeV]	9.46	9.86	9.89	9.91	10.02	10.23	10.26	10.27	10.36
ΔE [GeV]	1.10	0.70	0.67	0.64	0.53	0.34	0.30	0.29	0.20

Table 2: Bottomonium states and binding energies

Quarkonia are rather unusual hadrons. The masses of the light hadrons, in particular those of the non-strange mesons and baryons, arise almost entirely from the interaction energy of their nearly massless quark constituents. In contrast, the quarkonium masses are largely determined by the bare charm and bottom quark masses. These large quark masses allow a very straightforward calculation of many basic quarkonium properties, using non-relativistic potential theory. It is found that, in particular, the ground states and the lower

excitation levels of quarkonia are very much smaller than the normal hadrons, and that they are very tightly bound. Now deconfinement is a matter of scales: when the separation between normal hadrons becomes much less than the size of these hadrons, they melt to form the quark-gluon plasma. What happens at this point to the much smaller quarkonia? When do they become dissociated? That is the central theme of this report seen from another angle. We shall show that the disappearance of specific quarkonia signals the presence of a deconfined medium of a specific temperature [3]. Thus the study of the quarkonium spectrum in a given medium is akin to the spectral analysis of stellar media, where the presence or absence of specific excitation lines allows a determination of the temperature of the stellar interior.

The prediction of a new state of strongly interacting matter led quite naturally to the question of where and how to observe it. The very early universe is an obvious case: according to the usual evolution equations, giving its energy density as function of age, it must have been a quark-gluon plasma in the first 10 μs after the big bang. The core of neutron stars is another possibility, and they may in fact consist of deconfined quarks. But the essential boost for the field came from the idea to use high energy nuclear collisions to form small and short-lived bubbles of the quark-gluon plasma in the laboratory, making them accessible to terrestrial experimental study. This idea clearly contains assumptions to be verified, and we shall return to its basis later on. Here we only note that again an absolutely crucial question is how to probe the thermal conditions of the medium formed in such collisions. In view of the evolution of such a medium, this is a much more complex question than that addressed in the case of a box containing equilibrated strongly interacting matter. Nevertheless, as we shall see, quarkonia may well provide a tool for this more general task as well.

After this introduction, we shall first review the essential aspects of deconfinement (section 2.) and then summarize the basic properties of quarkonia and the dynamics of their dissociation (section 3.). Following this, we survey different approaches to quarkonium binding in QCD thermodynamics (section 4.). We then review the main theoretical features of quarkonium production in elementary as well as $p-A$ and nucleus-nucleus collisions (section 5.), and finally we try to see what one can learn from the present experimental results (section 6.).

2. Colour Deconfinement

The transition from hadronic matter to a plasma of deconfined quarks and gluons has been studied extensively in finite temperature lattice QCD. We shall consider here the case of vanishing baryon-number density (baryons and antibaryons in equal numbers) and comment only briefly on the situation at finite baryon density at the end of this section. At the transition point, the energy density of the system increases by the latent heat of deconfinement, i.e., it grows from a value determined by the degrees of freedom of a hadron gas to a much higher one governed by the degrees of freedom of a quark-gluon plasma. To illustrate this, we recall that the energy density of an ideal gas of massless pions is

$$\epsilon_\pi = 3 \frac{\pi^2}{30} T^4 \simeq T^4, \quad (1)$$

corresponding to the three possible pion charges, while an ideal quark-gluon plasma, with two massless quark flavours, gives

$$\epsilon_{QGP} = \left\{ 2 \times 8 + \frac{7}{8} [2 \times 2 \times 2 \times 3] \right\} \frac{\pi^2}{30} T^4 = 37 \frac{\pi^2}{30} T^4 \simeq 12 T^4, \quad (2)$$

as determined by the 16 gluonic and 24 quark-antiquark degrees of freedom. Hence in the vicinity of $T = T_c$, the energy density increases by more than a factor ten. The actual behaviour, as obtained in finite temperature lattice QCD for different flavour compositions [4, 5], is shown in Fig. 1.

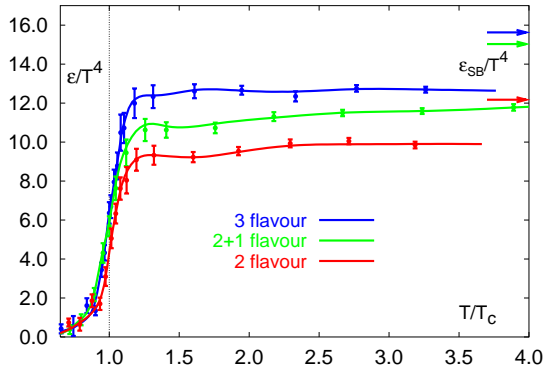


Figure 1: Energy density vs. T [4, 5]

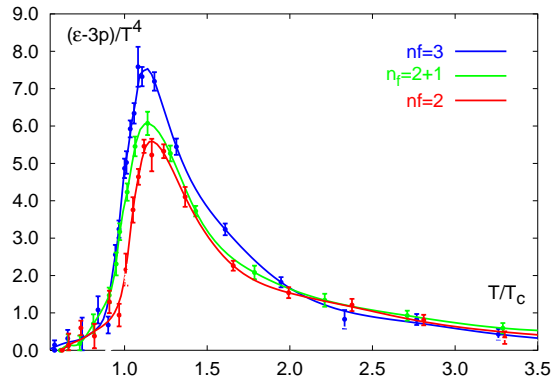


Figure 2: $\Delta = (\epsilon - 3P)/T^4$ vs. T [6]

Above T_c , the medium consists of deconfined quarks and gluons. We emphasize that deconfinement does not imply the absence of interaction – it is only the requirement to form colour neutral bound states that has been removed. In Fig. 2 it is seen that up to $T \sim 3 T_c$ the ‘interaction measure’ $\Delta = (\epsilon - 3P)/T^4$ remains sizeable and does not vanish [6], as it would for an ideal gas of massless constituents. This strong interaction in the quark-gluon plasma has been interpreted in various ways, as gradual onset of deconfinement starting from high momenta [7], as difference between physical and perturbative vacua [8], and even in terms of a large number of coloured “resonance” states [9]. Recent studies of the relevant degrees of freedom in the quark-gluon plasma [10] seem to indicate, however, that a description based on quarks having some kind of thermal mass is more likely to be correct.

To specify the nature of the critical behaviour observed at the transition, recall that in the limit of large quark mass ($m_q \rightarrow \infty$) we recover pure gauge theory and the average value of the Polyakov loop,

$$L(T) \sim \exp\{-F_{Q\bar{Q}}/T\}, \quad (3)$$

serves as order parameter [11]. Here

$$F_{Q\bar{Q}} = \lim_{r \rightarrow \infty} F_{Q\bar{Q}}(r, T) \quad (4)$$

denotes the large distance limit of the free energy of a heavy quark-antiquark pair, which diverges in the confined regime and becomes finite through colour screening in the quark-gluon plasma,

$$L(T) \begin{cases} = 0 & T \leq T_L \text{ confinement} \\ \neq 0 & T > T_L \text{ deconfinement} \end{cases} \quad (5)$$

This defines a critical deconfinement temperature T_L , separating the confined and deconfined phases. The underlying mechanism for such behaviour is a global Z_3 invariance of the Lagrangian of pure $SU(3)$ gauge theory, which becomes spontaneously broken in the deconfined phase, for $T \geq T_L$.

In the other extreme, the chiral limit of massless quarks ($m_q \rightarrow 0$), the QCD Lagrangian is chirally symmetric, and the chiral condensate

$$\chi(T) \equiv \langle \bar{\psi}\psi \rangle \quad (6)$$

serves as order parameter. At low temperatures, the massless quarks acquire an effective mass by dressing with gluons, so that the chiral symmetry is spontaneously broken. At high temperatures, thermal motion removes the dressing, so that the behaviour of $\chi(T)$,

$$\chi(T) \begin{cases} \neq 0 & T < T_\chi \text{ chiral symmetry broken} \\ = 0 & T \geq T_\chi \text{ chiral symmetry restored,} \end{cases} \quad (7)$$

defines a chiral restoration temperature T_χ separating the phases of broken and restored chiral symmetry.

While there thus exists well-defined thermal critical behaviour in the two limits of large and small quark mass, the QCD Lagrangian has for general finite quark masses neither a global Z_3 (deconfinement) nor a chiral symmetry. Nevertheless it is found that both the Polyakov loop and the chiral condensate continue to vary rapidly in the same narrow temperature interval, as shown in Fig. 3 for the case of two relatively light quark flavours [12]. We can thus still identify an “almost critical” behaviour, the so-called “rapid cross-over”. Since this occurs for $L(T)$ and $\chi(T)$ at the same temperature, deconfinement and chiral symmetry restoration are said to coincide.

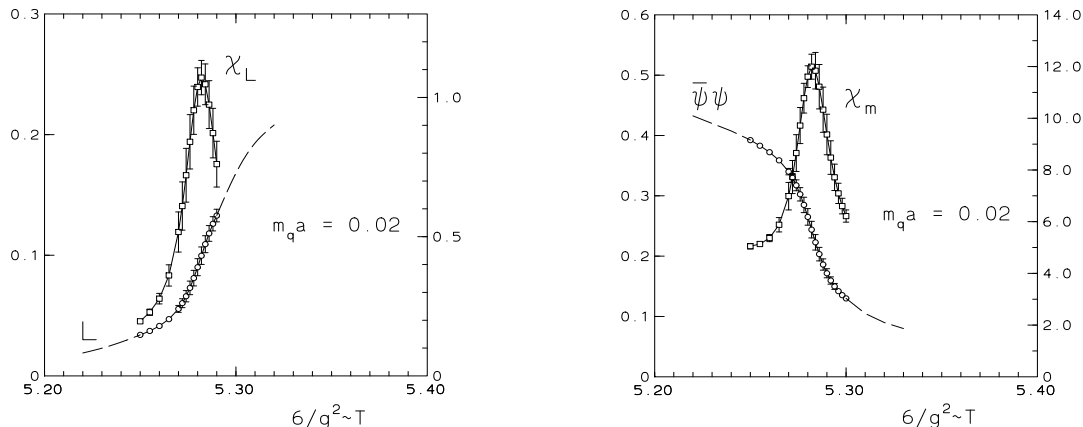


Figure 3: Polyakov loop and chiral condensate vs. temperature [12]

The “critical temperature” determined in this way depends on the masses and the number of quark flavours. For two light as well as for two light plus one heavier quark flavour, most studies [13] indicate $T_c = 175 \pm 10$ MeV, as shown in Fig. 4, although some indications for a higher value were recently reported [14].

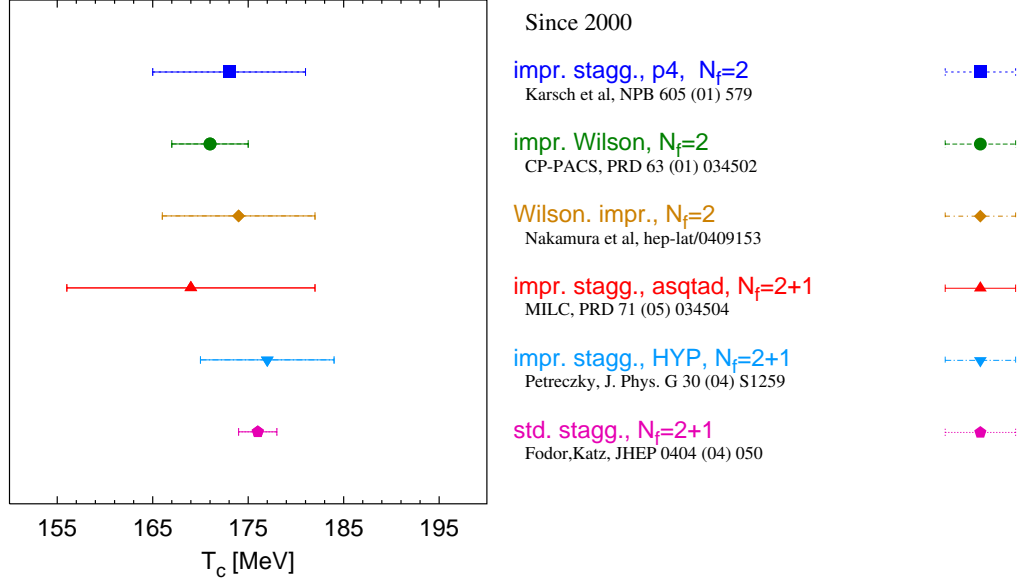


Figure 4: Critical temperature results from different lattice studies [13]

The precise form of critical behaviour in the limiting cases also depends on the number of colours and flavours. The situation is illustrated in Fig. 5 for colour $SU(3)$ and three quark flavours (u, d, s). In the gauge theory limit $m_q \rightarrow \infty$ for all flavours, the transition is discontinuous (first order). Decreasing the quark mass decreases the discontinuity, until it vanishes on a line of second order transitions, beyond which there is the rapid cross-over region. For three massless flavours, the chiral transition is also first order, and increasing the quark mass leads again to a decreasing discontinuity and a line of second order transitions. For two massless quark flavours and a sufficiently massive third flavour, the transition is of second order up to the two-flavour limit. The “physical point” corresponding to two light u and d quarks and one heavier s quark has now been established with some certainty and appears to fall into the cross-over region.

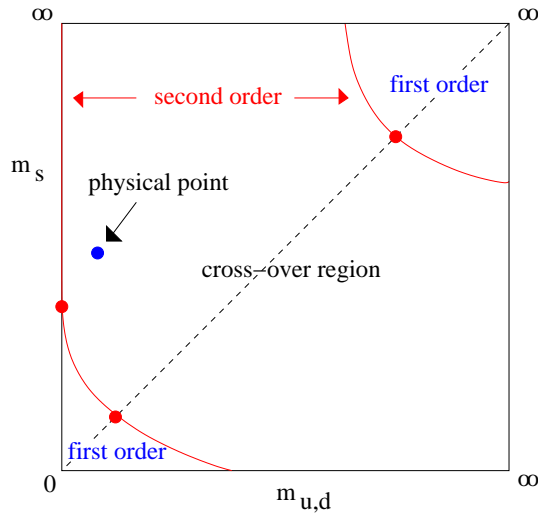


Figure 5: Critical behaviour as function of quark masses

The phase structure at non-vanishing baryon density has stimulated much interest [16], but it encounters calculational problems in the computer simulation. Quite recently, a number of methods to overcome these have been put forward [15], and today we believe that the phase diagram in T, μ has the form shown in Fig. 6, with μ denoting the baryochemical potential.

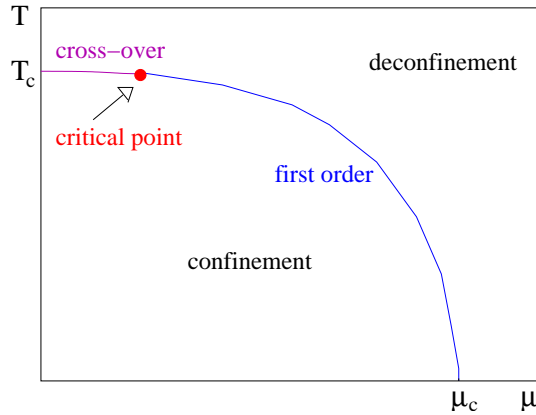


Figure 6: Critical behaviour for two light quark flavours, as function of T and μ

We can thus conclude this section by noting that the thermodynamics of strongly interacting matter is today known in considerable quantitative detail, with deconfinement for $\mu = 0$ setting in at $T_c = 175 \pm 10$ MeV. The actual nature of the “transition” remains, however, quite enigmatic, since it occurs as “rapid cross-over” and not as a genuine thermal phase transition. Further clarification could come from studies in the context of geometric critical behaviour, relating the onset of deconfinement to cluster formation and percolation.

Hence we know that confined hadronic and deconfined quark-gluon states of matter exist. How can we probe strongly interacting matter through specific observables, in order to determine its thermal parameters (temperature, energy density) as well as to identify its confinement status? Since we want to show that this can be done with the help of quarkonium states, we first summarize in the next section the essentials of quarkonium binding and break-up.

3. Quarkonium Binding and Dissociation

We had defined quarkonia as bound states of heavy quarks which are stable under strong decay, i.e., $M_{c\bar{c}} \leq 2M_D$ for charmonia and $M_{b\bar{b}} \leq 2M_B$ for bottomonia. Since the quarks are heavy, with $m_c \simeq 1.2 - 1.5$ GeV for the charm and $m_b \simeq 4.5 - 4.8$ GeV for the bottom quark, quarkonium spectroscopy can be studied quite well in non-relativistic potential theory. The simplest (“Cornell”) confining potential [17] for a $Q\bar{Q}$ at separation distance r has the form

$$V(r) = \sigma r - \frac{\alpha}{r} \quad (8)$$

with a string tension $\sigma \simeq 0.2$ GeV² and a Coulomb-like term with a gauge coupling

$\alpha \simeq \pi/12$. The corresponding Schrödinger equation

$$\left\{ 2m_c - \frac{1}{m_c} \nabla^2 + V(r) \right\} \Phi_i(r) = M_i \Phi_i(r) \quad (9)$$

then determines the bound state masses M_i and the wave functions $\Phi_i(r)$, and with

$$\langle r_i^2 \rangle = \int d^3r r^2 |\Phi_i(r)|^2 / \int d^3r |\Phi_i(r)|^2. \quad (10)$$

the latter in turn provide the (squared) average bound state radii.

To obtain a first idea of the results, we consider the semi-classical solution obtained by making use of the uncertainty relation $\langle p^2 \rangle \langle r^2 \rangle \simeq 1$ in the expression for the $Q\bar{Q}$ energy

$$E(r) = 2m + \frac{p^2}{m} + V(r) \simeq 2m + \frac{1}{mr^2} + V(r). \quad (11)$$

Minimizing $E(r)$ with respect to r , $dE/dr = 0$, gives

$$r_0 \simeq 0.44 \text{ fm} \Rightarrow M_0 = E(r_0) \simeq 3.1 \text{ GeV} \quad (12)$$

for the generic charmonium ground state, and

$$r_0 \simeq 0.33 \text{ fm} \Rightarrow M_0 = E(r_0) \simeq 9.6 \text{ GeV} \quad (13)$$

and for the corresponding bottomonium state. Here r_0 specifies the $Q\bar{Q}$ separation distances, i.e., it gives twice the radius. From Tables 1 and 2 we see that these first estimates already reproduce quite well the spin-averaged ground states.

The exact solution of eq. (9) gives in fact a very good account of the full (spin-averaged) quarkonium spectroscopy, as seen in Table 3 [19]. The line labelled ΔM shows the differences between the experimental and the calculated values; they are in all cases less than 1 %. Again r_0 gives the $Q\bar{Q}$ separation for the state in question. The input parameters for these results are $m_c = 1.25 \text{ GeV}$, $m_b = 4.65 \text{ GeV}$, $\sqrt{\sigma} = 0.445 \text{ GeV}$, $\alpha = \pi/12$.

state	J/ψ	χ_c	ψ'	Υ	χ_b	Υ'	χ'_b	Υ''
mass [GeV]	3.10	3.53	3.68	9.46	9.99	10.02	10.26	10.36
ΔE [GeV]	0.64	0.20	0.05	1.10	0.67	0.54	0.31	0.20
ΔM [GeV]	0.02	-0.03	0.03	0.06	-0.06	-0.06	-0.08	-0.07
r_0 [fm]	0.50	0.72	0.90	0.28	0.44	0.56	0.68	0.78

Table 3: Quarkonium Spectroscopy from Non-Relativistic Potential Theory [19]

We thus see that in particular the J/ψ and the lower-lying bottomonium states are very tightly bound ($2M_{D,B} - M_0 \gg l$) and of very small spatial size ($r_0 \ll 2r_h \simeq 2 \text{ fm}$). Through what kind of interaction dynamics can they then be dissociated?

As illustration, we consider the collision dissociation of a J/ψ . It is very small ($r_{J/\psi} \sim 0.25$ fm) and hence can only be resolved by a sufficiently hard probe. It is moreover tightly bound ($2M_D - M_{J/\psi} \sim 0.6$ GeV), so that only a sufficiently energetic projectile can break the binding. Hence in a collision with a normal hadron, the J/ψ can only be dissociated by an interaction with a hard gluon constituent of the hadron, not with the hadron as a whole (see Fig. 7).

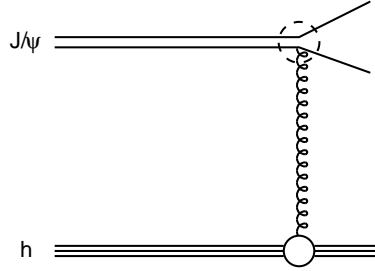


Figure 7: J/ψ -hadron interaction

The gluon momentum distribution $g(x)$ in a hadron is determined in deep inelastic lepton-hadron scattering; with k_h denoting the gluon momentum, $x = k_h/p_h$ specifies the fraction of the incident hadron momentum p_h carried by the gluon. For mesons, one finds for large momenta

$$g(x) \sim (1-x)^3, \quad (14)$$

so that the average momentum of a hadronic gluon is

$$\langle k \rangle_h = \frac{1}{5} \langle p_h \rangle. \quad (15)$$

For thermal hadrons in confined matter, $\langle p_h \rangle \sim 3T$, with $T < 175$ MeV, so that with

$$\langle k \rangle_h = \frac{3}{5} T \leq 0.1 \text{ GeV} \ll 0.6 \text{ GeV} \quad (16)$$

the gluon momentum is far too low to allow a dissociation of the J/ψ .

On the other hand, the average momentum of a deconfined thermal gluon in a quark-gluon plasma will be

$$\langle k_g \rangle \simeq 3 T \quad (17)$$

and for $T > 1.15 T_c$, this provides enough energy to overcome the J/ψ binding. We thus expect that a hot deconfined medium can lead to J/ψ dissociation, while the gluons available in a confined medium are too soft to allow this.

To make these considerations quantitative, one first has to calculate the cross-section for the gluon-dissociation of a J/ψ , a QCD analogue of the photo-effect. This can be carried out using the operator product expansion [20, 21], and the result is

$$\sigma_{g-J/\psi} \sim \frac{1}{m_c^2} \frac{(k/\Delta E_\psi - 1)^{3/2}}{(k/\Delta E_\psi)^5} \quad (18)$$

with $\Delta E_{J/\psi} = 2M_D - M_{J/\psi}$. The corresponding cross-section for the hadron dissociation is then obtained by convoluting the gluon-dissociation cross-section (18) with the hadronic gluon distribution function $g(x)$, which for J/ψ -meson interactions leads to

$$\sigma_{h-J/\psi} \simeq \sigma_{\text{geom}}(1 - \lambda_0/\lambda)^{5.5} \quad (19)$$

with $\lambda \simeq (s - M_\psi^2)/M_\psi$ and $\lambda_0 \simeq (M_h + \Delta E_\psi)$. Here $\sigma_{\text{geom}} \simeq \pi r_{J/\psi}^2 \simeq 2$ mb is the geometric J/ψ cross-section and M_h denotes the mass of the incident meson. In Fig. 8, we compare the two dissociation cross-sections (18) and (19) as function of the incident projectile momentum.

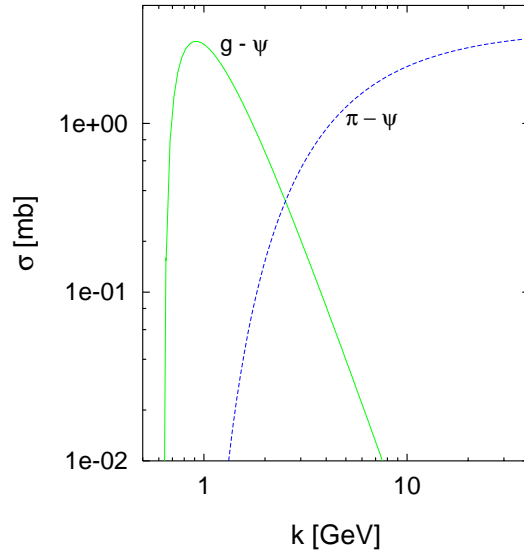


Figure 8: Gluon and hadron J/ψ dissociation cross-sections [21]

This result confirms the qualitative arguments given at the beginning of this section: typical thermal gluon momenta near 1 GeV produce a large dissociation cross-section, whereas hadron momenta in a thermal range (up to 2 - 3 GeV) still lead to a vanishingly small cross-section. In other words, the J/ψ should survive in confining media, but become dissociated in a hot quark-gluon plasma.

The calculations leading to eq. (18) are exact in the large quark mass limit $m_Q \rightarrow \infty$. It is not clear if the charm quark mass really satisfies this condition, and so the dissociation cross section in J/ψ -hadron collisions has been discussed in other approaches, some of which lead to much larger values [22]. The basic question is apparently whether or not the charmonium wave function has enough overlap with that of the usual hadrons to lead to a sizeable effect. It may well be that this question is resolvable only experimentally, by testing if slow charmonia in normal nuclear matter suffer significant dissociation. Such experiments are definitely possible [23].

4. Thermal Quarkonium Dissociation

We shall here address the first of our “basic” questions: how can we identify through measurements the states of matter in a fully equilibrated QCD medium? Assume that

we are given a box of such strongly interacting matter, in a stationary state of thermal equilibrium at a given temperature. Is it possible to specify the state of the given matter and transitions between different states in terms of observable quantities calculated in QCD?

4.1 Interaction Range and Colour Screening

Consider a colour-singlet bound state of a heavy quark Q and its antiquark \bar{Q} , put into the medium in such a way that we can measure the energy of the system as function of the $Q\bar{Q}$ separation r (see Fig. 9). The quarks are assumed to be heavy so that they are static and any energy changes indicate changes in the binding energy. We consider first the case of vanishing baryon density; at $T = 0$, the box is therefore empty.

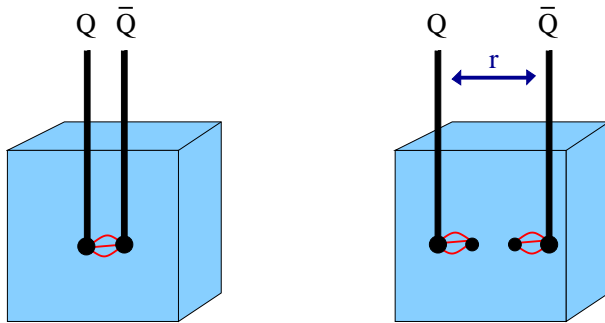


Figure 9: String breaking for a $Q\bar{Q}$ system

In vacuum, i.e., at $T = 0$, the free energy of the $Q\bar{Q}$ pair is assumed to have the string form [17]

$$F(r) \sim \sigma r \quad (20)$$

where $\sigma \simeq 0.16 \text{ GeV}^2$ is the string tension as determined in the spectroscopy of heavy quark resonances (charmonium and bottomonium states). Thus $F(r)$ increases with separation distance; but when it reaches the value of a pair of dressed light quarks (about the mass of a ρ meson), it becomes energetically favorable to produce a $q\bar{q}$ pair from the vacuum, break the string and form two light-heavy mesons ($Q\bar{q}$) and ($\bar{Q}q$). These can now be separated arbitrarily far without changing the energy of the system (Fig. 9).

The string breaking energy for charm quarks is found to be

$$F_0 = 2(M_D - m_c) \simeq 1.2 \text{ GeV}; \quad (21)$$

for bottom quarks, one obtains the same value,

$$F_0 = 2(M_B - m_b) \simeq 1.2 \text{ GeV}, \quad (22)$$

using in both cases the quark mass values obtained in the solution leading to Table 3. Hence the onset of string breaking is evidently a property of the vacuum as a medium. It occurs when the two heavy quarks are separated by a distance

$$r_0 \simeq 1.2 \text{ GeV}/\sigma \simeq 1.5 \text{ fm}, \quad (23)$$

independent of the mass of the (heavy) quarks connected by the string.

If we heat the system to get $T > 0$, the medium begins to contain light mesons, and the large distance $Q\bar{Q}$ potential $F(\infty, T)$ decreases, since we can use these light hadrons to achieve an earlier string breaking through a kind of flip-flop recoupling of quark constituents [24], resulting in an effective screening of the interquark force (see Fig. 10). Near the deconfinement point, the hadron density increases rapidly, and hence the recoupling dissociation becomes much more effective, causing a considerable decrease of $F(\infty, T)$.

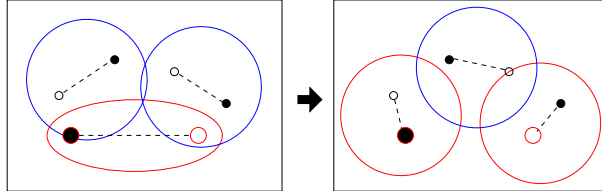


Figure 10: In-medium string breaking through recoupling

A further increase of T will eventually bring the medium to the deconfinement point T_c , at which chiral symmetry restoration causes a rather abrupt drop of the light quark dressing (equivalently, of the constituent quark mass), increasing strongly the density of constituents. As a consequence, $F(\infty, T)$ now continues to drop sharply. Above T_c , light quarks and gluons become deconfined colour charges, and this quark-gluon plasma leads to a colour screening, which limits the range of the strong interaction. The colour screening radius r_D , which determines this range, is inversely proportional to the density of charges, so that it decreases with increasing temperature. As a result, the $Q\bar{Q}$ interaction becomes more and more short-ranged.

In summary, starting from $T = 0$, the $Q\bar{Q}$ probe first tests vacuum string breaking, then a screening-like dissociation through recoupling of constituent quarks, and finally genuine colour screening. In Fig. 11, we show the behaviour obtained in full two-flavour QCD for the colour-singlet $Q\bar{Q}$ free energy as a function of r for different T [25].

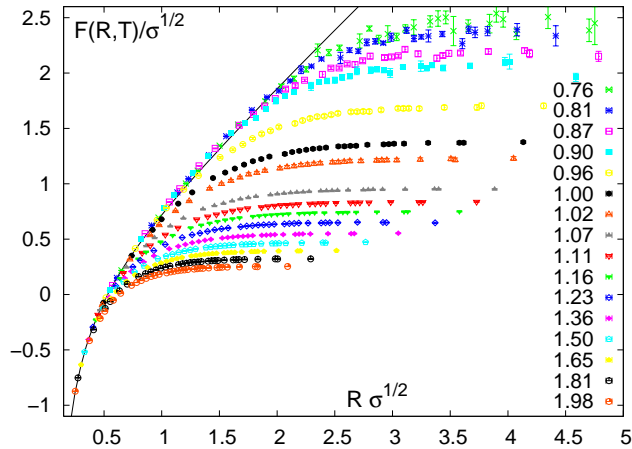


Figure 11: The colour singlet $Q\bar{Q}$ free energy $F(r, T)$ vs. r at different T [25]

It is evident in Fig. 11 that the asymptotic value $F(\infty, T)$, i.e., the energy needed to separate the $Q\bar{Q}$ pair, decreases with increasing temperature, as does the separation distance at which “the string breaks”. For the moment we consider the latter to be defined by the point beyond which the free energy remains constant within errors, returning in section 4.3 to a more precise definition. The behaviour of both quantities is shown in Fig. 12. Deconfinement is thus reflected very clearly in the temperature behaviour of the heavy quark potential: both the string breaking energy and the interaction range drop sharply around T_c . The latter decreases from hadronic size in the confinement region to much smaller values in the deconfined medium, where colour screening is operative.

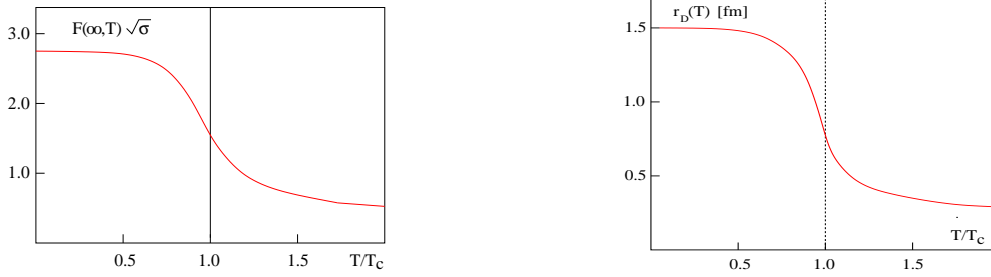


Figure 12: String breaking potential and interaction range at different temperatures

The in-medium behaviour of heavy quark bound states thus does serve quite well as probe of the state of matter in QCD thermodynamics. We had so far just considered $Q\bar{Q}$ bound states in general. Let us now turn to a specific state such as the J/ψ . What happens when the range of the binding force becomes smaller than the radius of the state? Since the c and the \bar{c} can now no longer see each other, the J/ψ must dissociate for temperatures above this point. Hence the dissociation points of the different quarkonium states provide a way to measure the temperature of the medium. The effect is illustrated schematically in Fig. 13, showing how with increasing temperature the different charmonium states “melt” sequentially as function of their binding strength; the most loosely bound state disappears first, the ground state last.

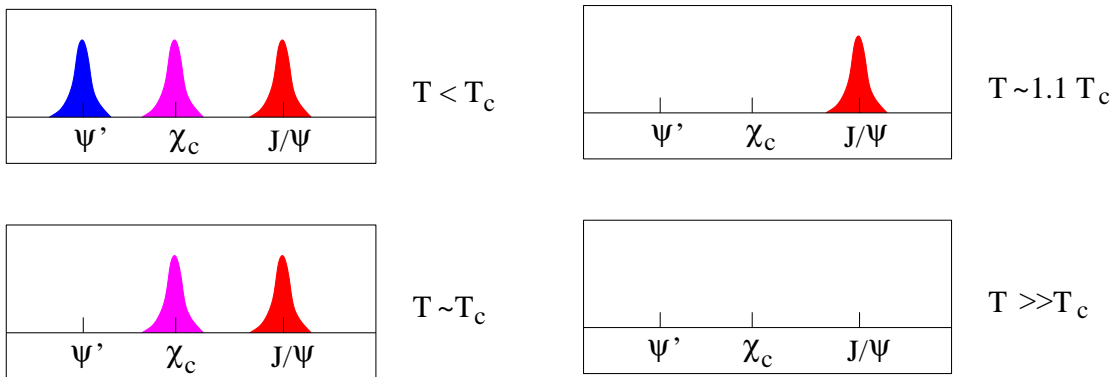


Figure 13: Charmonium spectra at different temperatures

Moreover, since finite temperature lattice QCD also provides the temperature dependence of the energy density, the melting of the different charmonia or bottomonia can be specified

as well in terms of ϵ . In Fig 14, we illustrate this, combining the the energy density from Fig. 1 and the force radii from Fig. 12. It is evident that although ψ' and χ_c are expected to melt around T_c , the corresponding dissociation energy densities will presumably be quite different.

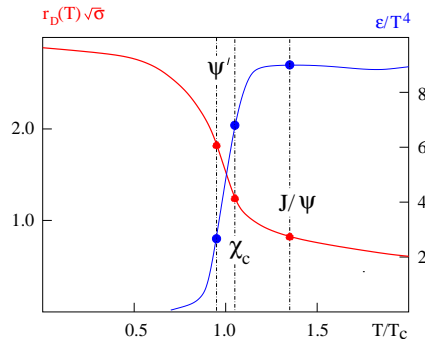


Figure 14: Charmonium dissociation vs. temperature and energy density

To make these considerations quantitative, we thus have to find a way to determine the in-medium melting points of the different quarkonium states. This problem has been addressed in three different approaches:

- Model the heavy quark potential as function of the temperature, $V(r, T)$, and solve the resulting Schrödinger equation (9).
- Determine the internal energy $U(r, T)$ of a $Q\bar{Q}$ pair at separation distance r from lattice results for the corresponding free energy $F(r, T)$, using the thermodynamic relation

$$U(r, T) = -T^2 \left(\frac{\partial[F(r, T)/T]}{\partial T} \right) = F(r, T) - T \left(\frac{\partial F(r, T)}{\partial T} \right), \quad (24)$$

and solve the Schrödinger equation with $V(r, T) = U(r, T)$ as the binding potential.

- Calculate the quarkonium spectrum directly in finite temperature lattice QCD.

Clearly the last is the only model-independent way, and it will in the long run provide the decisive determination. However, the direct lattice study of charmonium spectra has become possible only quite recently, and so far only in quenched QCD (no dynamical light quarks); corresponding studies for bottomonia are still more difficult. Hence much of what is known so far is based on Schrödinger equation studies with different model inputs. To illustrate the model-dependence of the dissociation parameters, we first cite some early work using different models for the temperature dependence of $V(r, T)$, then some recent studies based on lattice results for $F(r, T)$, and finally summarize the present state of direct lattice calculations of charmonia in finite temperature media.

4.2 Potential Model Studies

The first quantitative studies of finite temperature charmonium dissociation [26] were based on screening in the form obtained in one-dimensional QED, the so-called Schwinger

model. The confining part of the Cornell potential (8), $V(r) \sim \sigma r$, is the solution of the Laplace equation in one space dimension. In this case, Debye-screening leads to [27]

$$V(r, T) \sim \sigma r \left\{ \frac{1 - e^{-\mu r}}{\mu r} \right\}, \quad (25)$$

where $\mu(T)$ denotes the screening mass (inverse Debye radius) for the medium at temperature T . This form reproduces at least qualitatively the convergence to a finite large distance value $V(\infty, T) = \sigma/\mu(T)$, and since $\mu(T)$ increases with T , it also gives the expected decrease of the potential with increasing temperature. Combining this with the usual Debye screening for the $1/r$ part of eq. (8) then leads to

$$V(r, T) \sim \sigma r \left\{ \frac{1 - e^{-\mu r}}{\mu r} \right\} - \frac{\alpha}{r} e^{-\mu r} = \frac{\sigma}{\mu} \left\{ 1 - e^{-\mu r} \right\} - \frac{\alpha}{r} e^{-\mu r} \quad (26)$$

for the screened Cornell potential. In [26], the screening mass was assumed to have the form $\mu(T) \simeq 4 T$, as obtained in first lattice estimates of screening in high temperature $SU(N)$ gauge theory. Solving the Schrödinger equation with these inputs, one found that both the ψ' and the χ_c become dissociated essentially at $T \simeq T_c$, while the J/ψ persisted up to about $1.2 T_c$. Note that as function of the energy density $\epsilon \sim T^4$, this meant that the J/ψ really survives up to much higher ϵ .

This approach has two basic shortcomings:

- The Schwinger form (25) corresponds to the screening of σr in one space dimension; the correct result in three space dimensions is different [27].
- The screening mass $\mu(T)$ is assumed in its high energy form; lattice studies show today that its behaviour near T_c is quite different [28].

While the overall behaviour of this approach provides some first insight into the problem, quantitative aspects require a more careful treatment.

When lattice results for the heavy quark free energy as function of the temperature first became available, an alternative description appeared [29]. It assumed that in the thermodynamic relation (24) the entropy term $-T(\partial F/\partial T)$ could be neglected, thus equating binding potential and free energy,

$$V(r, T) = F(r, T) - T(\partial F/\partial T) \simeq F(r, T). \quad (27)$$

Using this potential in the Schrödinger equation (9) specifies the temperature dependence of the different charmonium masses. On the other hand, the large distance limit of $V(r, T)$ determines the temperature variation of the open charm meson D ,

$$2M_D(T) \simeq 2m_c + V(\infty, T) \quad (28)$$

In fig. 15, we compare the resulting open and hidden charm masses as function of temperature. It is seen that the ψ' mass falls below $2 M_D$ around $0.2 T_c$, that of the χ_c at about $0.8 T_c$; hence these states disappear by strong decay at the quoted temperatures. Only the ground state J/ψ survives up to T_c and perhaps slightly above; the lattice data available at the time did not extend above T_c , so further predictions were not possible.

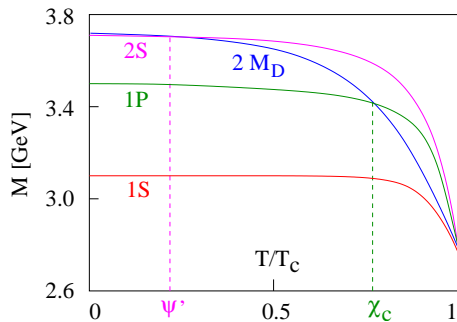


Figure 15: Temperature dependence of open and hidden charm masses [29]

The main shortcoming of this approach is quite evident. The neglect of the entropy term in the potential reduces $V(r, T)$ and hence the binding. As a result, the D mass drops faster with temperature than that of the charmonium states, and it is this effect which leads to the early charmonium dissociation. Moreover, in the lattice studies used here, only the colour averaged free energy was calculated, which leads to a further reduction of the binding force.

We conclude from these attempts that for a quantitative potential theory study, the free energy has to be formulated in the correct three-dimensional screened Cornell form, and it then has to be checked against the space- and temperature-dependence of the corresponding colour singlet quantity obtained in lattice QCD.

4.3 Screening Theory

The modification of the interaction between two charges immersed in a dilute medium of charged constituents is provided by Debye-Hückel theory, which for the Coulomb potential in three space dimensions leads to the well-known Debye screening,

$$\frac{1}{r} \rightarrow \frac{1}{r} \epsilon^{-\mu r}, \quad (29)$$

where $r_D = 1/\mu$ defines the screening radius [30]. Screening can be evaluated more generally [27] for a given free energy $F(r) \sim r^q$ in d space dimensions, with an arbitrary number q . We shall here apply this to the two terms of the Cornell form, with $q = 1$ for the string term, $q = -1$ for the gauge term, in $d = 3$ space dimensions [28].

We thus assume that the screening effect can be calculated separately for each term, so that the screened free energy becomes

$$F(r, T) = F_s(r, T) + F_c(r, T) = \sigma r f_s(r, T) - \frac{\alpha}{r} f_c(r, T). \quad (30)$$

The screening functions $f_s(r, T)$ and $f_c(r, T)$ must satisfy

$$\begin{aligned} f_s(r, T) &= f_c(r, T) = 1 \quad \text{for } T \rightarrow 0, \\ f_s(r, T) &= f_c(r, T) = 1 \quad \text{for } r \rightarrow 0, \end{aligned} \quad (31)$$

since at $T = 0$ there is no medium, while in the short-distance limit $T^{-1} \gg r \rightarrow 0$, the medium has no effect. The resulting forms are [27]

$$F_c(r, T) = -\frac{\alpha}{r} \left[e^{-\mu r} + \mu r \right] \quad (32)$$

for the gauge term, and

$$F_s(r, T) = \frac{\sigma}{\mu} \left[\frac{\Gamma(1/4)}{2^{3/2}\Gamma(3/4)} - \frac{\sqrt{\mu r}}{2^{3/4}\Gamma(3/4)} K_{1/4}[(\mu r)^2] \right] \quad (33)$$

for the string term. The first term in eq. (33) gives the constant large distance limit due to colour screening; the second provides a Gaussian cut-off in $x = \mu r$, since $K_{1/4}(x^2) \sim \exp\{-x^2\}$, which is in contrast to the exponential cut-off given by the Schwinger form (26).

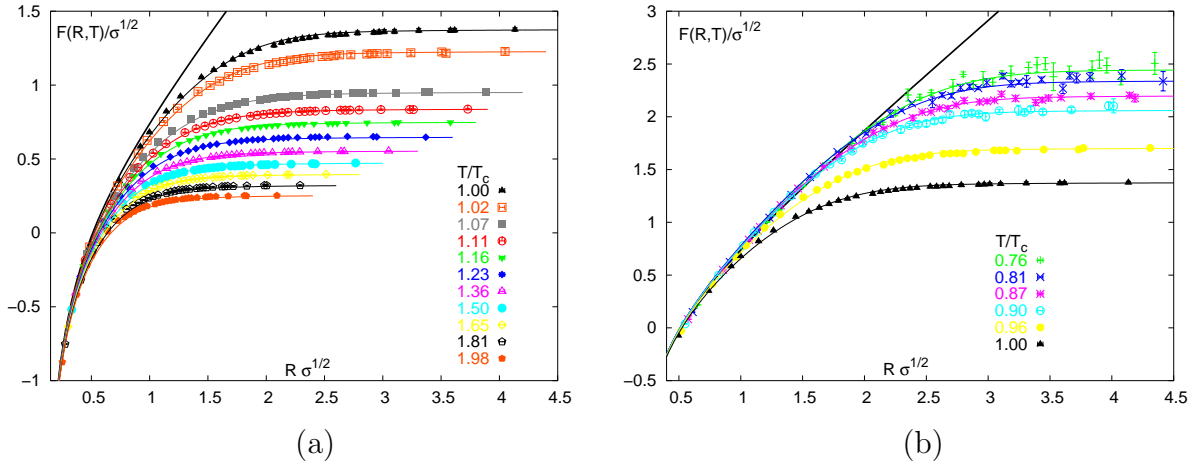


Figure 16: Screening fits to the $Q\bar{Q}$ free energy $F(r, T)$ for $T \geq T_c$ (left) and $T \leq T_c$ (right) [28]

At temperatures $T > T_c$, when the medium really consists of unbound colour charges, we thus expect the free energy $F(r, T)$ to have the form (30), with the two screened terms given by eqs. (32) and (33). In Fig. 16a, it is seen that the results for the colour singlet free energy calculated in two-flavour QCD [31] are indeed described very well by this form, with $m_c = 1.25$ GeV and $\sqrt{\sigma} = 0.445$ GeV, as above. The only parameter to be determined, the screening mass μ , is shown in Fig. 17, and as expected, it first increases rapidly in the transition region and then turns into the perturbative form $\mu \sim T$.

The behaviour of $Q\bar{Q}$ binding in a plasma of unbound quarks and gluons is thus well described by colour screening. Such a description is in fact found to work well also for $T < T_c$, when quark recombination leads to an effective screening-like reduction of the interaction range, provided one allows higher order contributions in $x = \mu r$ in the Bessel function $K_{1/4}(x^2)$ governing string screening [28]. The resulting fit to the two-flavour colour singlet free energy below T_c is shown in Fig. 16b, using $K_{1/4}(x^2 + (1/2)x^4)$ in eq. (33); the corresponding values for the screening mass are included in Fig. 17.

With the free energy $F(r, T)$ of a heavy quark-antiquark pair given in terms of the screening form obtained from Debye-Hückel theory, the internal energy $U(r, T)$ can now be obtained through the thermodynamic relation (24), and this then provides the binding potential $V(r, T)$ for the temperature dependent version of the Schrödinger equation (9). The resulting solution then specifies the temperature-dependence of charmonium binding as based on the correct heavy quark potential [19]. Let us briefly comment on the thermodynamic basis of this approach. The pressure P of a thermodynamic system is given

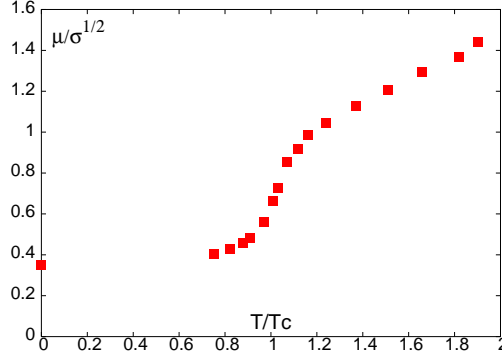


Figure 17: The screening mass $\mu(T)$ vs. T [28, 19]

by the free energy, $P = -F = -U + TS$; it is determined by the kinetic energy TS at temperature T and entropy $S(T)$, reduced by the potential energy $U(T)$ between the constituents. In our case, all quantities give the difference between a thermodynamic system containing a $Q\bar{Q}$ pair and the corresponding system without such a pair. The potential energy of the $Q\bar{Q}$ pair, due both to the attraction of Q and \bar{Q} and to the modification which the pair causes to the internal energy of the other constituents of the medium, is therefore given by U . To determine the dissociation points for the different quarkonium states, we thus have to solve the Schrödinger equation (9) with $V(r, T) = U(r, T)$.

From eqs. (32) and (33) we get for the $Q\bar{Q}$ potential

$$V(r, T) = V(\infty, T) + \tilde{V}(r, T), \quad (34)$$

with

$$V(\infty, T) = c_1 \frac{\sigma}{\mu} - \alpha\mu + T \frac{d\mu}{dT} \left[c_1 \frac{\sigma}{\mu^2} + \alpha \right], \quad (35)$$

and $c_1 = \Gamma(1/4)/2^{3/2}\Gamma(3/4)$, and where $\tilde{V}(r, T)$ contains the part of the potential which vanishes for $r \rightarrow \infty$. The behaviour of $V(\infty, T)$ as function of the temperature is shown in Fig. 18. It measures (twice) the energy of the cloud of light quarks and gluons around an isolated heavy quark, of an extension determined by the screening radius, relative to the energy contained in such a cloud of the same size without a heavy quark. This energy difference arises from the interaction of the heavy quark with light quarks and gluons of the medium, and from the modification of the interaction between the light constituents themselves, caused by the presence of the heavy charge. – The behaviour of $\tilde{V}(r, T)$ is shown in Fig. 19 for three different values of the temperature. It is seen that with increasing T , screening reduces the range of the potential.

The relevant Schrödinger equation now becomes

$$\left\{ -\frac{1}{m_c} \nabla^2 + \tilde{V}(r, T) \right\} \Phi_i(r) = \Delta E_i(T) \Phi_i(r) \quad (36)$$

where

$$\Delta E_i(T) = M_i - 2m_c - V(\infty, T) \quad (37)$$

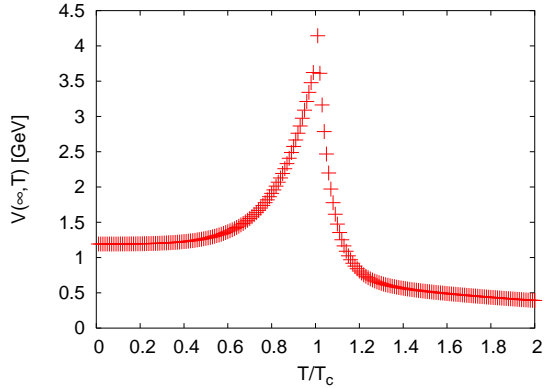


Figure 18: The large distance limit of the quarkonium potential $V(r, T)$ [19]

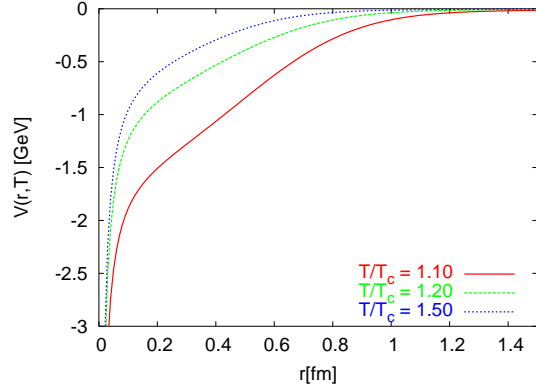


Figure 19: Variation of $\tilde{V}(r, T)$ with r for different T [19]

is the binding energy of charmonium state i at temperature T . When it vanishes, the bound state i no longer exists, so that $\Delta E_i(T) = 0$ determines the dissociation temperature T_i for that state. The temperature enters only through the T -dependence of the screening mass $\mu(T)$, as obtained from the analysis of the lattice results for $F(r, T)$. In Fig. 20, we show the resulting binding energy behaviour for the different charmonium states, obtained with $m_c = 1.25$ GeV and $\sqrt{\sigma} = 0.445$ GeV; in Fig. 21, we show the corresponding bound state radii [19]. It is seen that in particular the divergence of the radii defines quite well the different dissociation points.

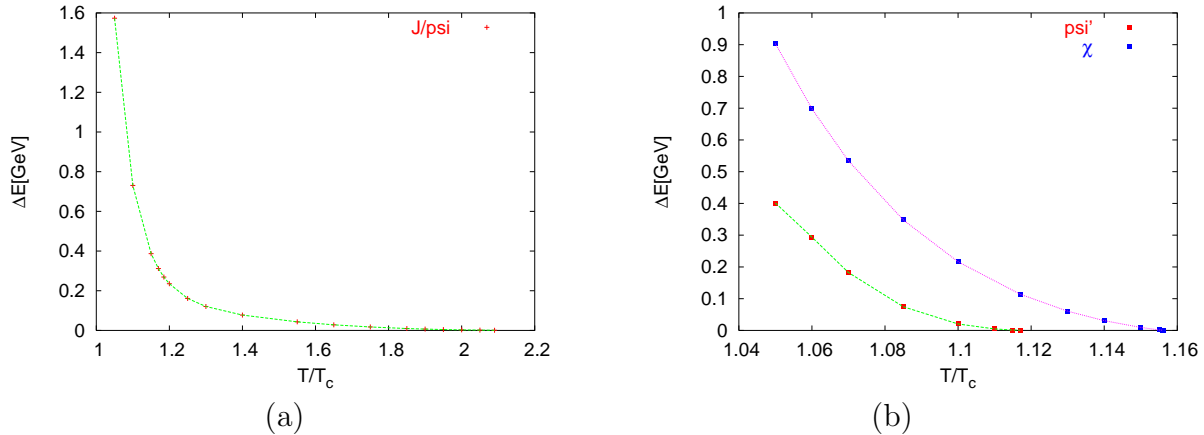


Figure 20: T -dependence of binding energy for J/ψ (a) and for χ_c / ψ' (b) [19]

The same formalism, with $m_b = 4.65$ GeV replacing m_c , leads to the bottomonium dissociation points. The combined quarkonium results are listed in Table 3. They agree quite well with those obtained in a very similar study based on corresponding free energies obtained in quenched lattice QCD [32], indicating that above T_c gluonic effects dominate. Using a parametrically generalized screened Coulomb potential obtained from lattice QCD results also leads to very compatible results for the $N_f = 2$ and quenched cases[33]. We recall here that the main underlying change, which is responsible for the much higher dissociation temperatures for the quarkonium ground states, is the use of

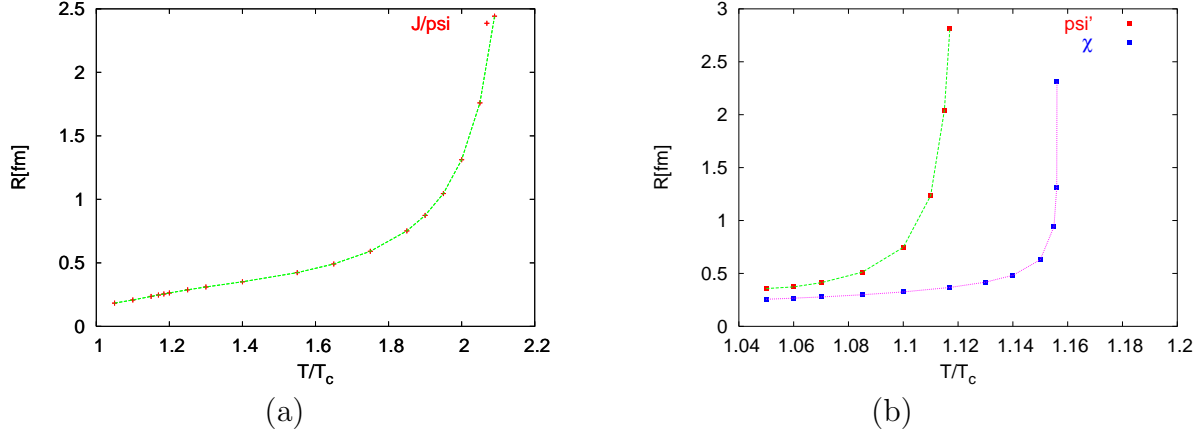


Figure 21: T -dependence of bound state radii for J/ψ (a) and for χ_c / ψ' (b) [19]

the full internal energy (24), including the entropy term, as potential in the Schrödinger equation: this makes the binding much stronger.

We should note, however, that in all such potential studies it is not so clear what binding energies of less than a few MeV or bound state radii of several fermi can mean in a medium whose temperature is above 200 MeV and which leads to screening radii of less than 0.5 fm. In such a situation, thermal activation [34] can easily dissociate the bound state.

state	$J/\psi(1S)$	$\chi_c(1P)$	$\psi'(2S)$	$\Upsilon(1S)$	$\chi_b(1P)$	$\Upsilon(2S)$	$\chi_b(2P)$	$\Upsilon(3S)$
T_d/T_c	2.10	1.16	1.12	> 4.0	1.76	1.60	1.19	1.17

Table 3: Quarkonium Dissociation Temperatures [19]

4.4 Charmonium Correlators

The direct spectral analysis of charmonia in finite temperature lattice has come within reach only in very recent years [35]. It is possible now to evaluate the correlation functions $G_H(\tau, T)$ for hadronic quantum number channels H in terms of the Euclidean time τ and the temperature T . These correlation functions are directly related to the corresponding spectral function $\sigma_H(M, T)$, which describe the distribution in mass M at temperature T for the channel in question. In Fig. 22, schematic results at different temperatures are shown for the J/ψ and the χ_c channels. It is seen that the spectrum for the ground state J/ψ remains essentially unchanged even at $1.5 T_c$. At $3 T_c$, however, it has disappeared; the remaining spectrum is that of the $c\bar{c}$ continuum of J/ψ quantum numbers at that temperature. In contrast, the χ_c is already absent at $1.1 T_c$, with only the corresponding continuum present.

These results are clearly very promising: they show that in a foreseeable future, the dissociation parameters of quarkonia can be determined *ab initio* in lattice QCD. For the moment, however, they remain indicative only, since the underlying calculations were

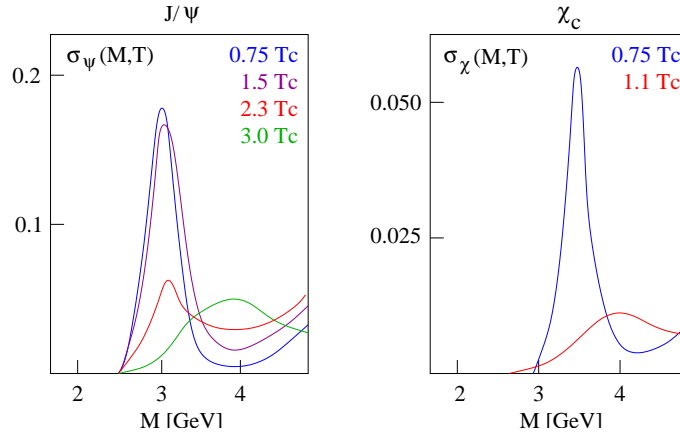


Figure 22: J/ψ and χ_c spectral functions at different temperatures

generally performed in quenched QCD, i.e., without dynamical quark loops. Since such loops are crucial in the break-up of quarkonia into light-heavy mesons, final results require calculations in full QCD. Some first calculations in two-flavour QCD have just appeared [36] and support the late dissociation of the J/ψ . The widths of the observed spectral signals are at present determined by the precision of the lattice calculations; to study the actual physical widths, much higher precision is needed. Finally, one has so far only first signals at a few selected points; a temperature scan also requires higher performance computational facilities. Since the next generation of computers, in the multi-Teraflops range, is presently going into operation, the next years should bring the desired results. So far, in view of the mentioned uncertainties in both approaches, the results from direct lattice studies and those from the potential model calculations of the previous section appear quite compatible.

5. Quarkonium Production in Nuclear Collisions

The aim of high energy nuclear collisions is to study colour deconfinement and the resulting quark-gluon plasma in the laboratory. Here we want to show how quarkonia can be used as a probe in this study. The medium to be probed as well as the quarkonium probes are produced in the collision, so that we have to address evolution aspects in both cases. After a brief section on the evolution of nuclear collisions, we shall first consider quarkonium formation in elementary proton-proton collisions and then turn to in-medium phenomena of quarkonia in nuclear collisions.

5.1 Nuclear Collisions

Starting from the non-equilibrium configuration of two colliding nuclei, the evolution of the collision is assumed to have the form shown in Fig. 23. After the collision, there is a short pre-equilibrium stage, in which the primary partons of the colliding nuclei interact and thermalize to form the quark-gluon plasma. This then expands, cools and hadronizes. The partonic constituents in the initial state of the collision are given by the parton distribution functions of the colliding nuclei. To produce a large-scale thermal system, partons from different nucleon-nucleon collisions have to undergo multiple interactions. In the cen-

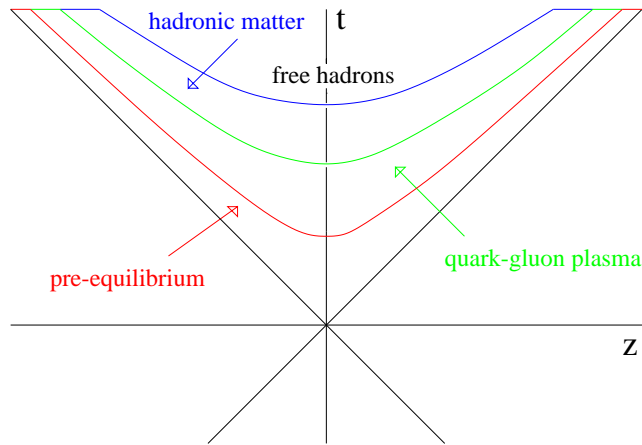


Figure 23: Expected evolution of a nuclear collision

ter of mass of a high energy collision, the incoming nuclei are strongly Lorentz-contracted; the resulting parton distribution in the transverse collision plane is schematically illustrated in Fig. 24. The transverse size of the partons is determined by their intrinsic transverse momentum, and the number of partons contained in a nucleon is known from deep inelastic scattering experiments. The density of partons increases with both A and \sqrt{s} , and at some critical point, parton percolation occurs [37] and global colour connection sets in. In the resulting connected medium, partons lose their independent existence and well-defined origin, so that there is deconfinement, but not yet thermalization. In recent years, such partonic connectivity requirements (parton saturation, colour glass condensate) have attracted much attention [37, 38]; they appear to form a prerequisite for subsequent thermalization.

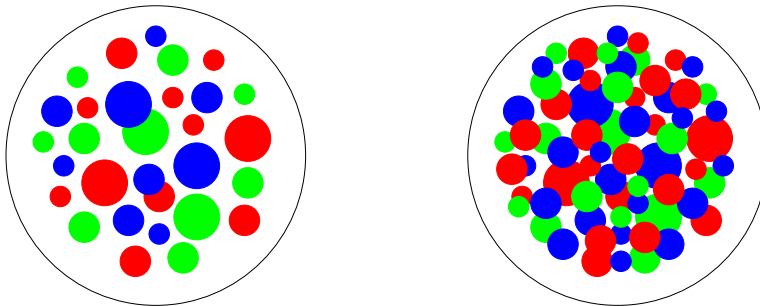


Figure 24: Parton distributions in the transverse plane of a nucleus-nucleus collision

Assuming that after an equilibration time τ_0 a thermalized plasma of deconfined (but interacting) quarks and gluons is formed, the initial energy density of the medium can be estimated in terms of the emitted hadrons and the initial interaction volume [39]

$$\epsilon = \left(\frac{dN_h}{dy} \right)_{y=0} \frac{w_h}{\pi R_A^2 \tau_0}, \quad (38)$$

where $(dN_h/dy)_{y=0}$ specifies the number of hadrons emitted in the nuclear collision per unit rapidity at mid-rapidity, and w_h their average energy. The initial transverse size is

determined by the nuclear radius R_A , or the nuclear overlap area in non-central collisions. The initial longitudinal extension is governed by the equilibration time, which was originally taken to be about 1 fm [39]. This appears quite reasonable in media, in which the intrinsic QCD scale $l^{-1} \simeq 1$ fm is the relevant measure. For denser partonic systems, one can expect a faster thermalization, and so it seems meaningful to use the parton density to scale τ_0 to higher collision energies. The number of partons emitted by a colliding nucleon is about two at SPS energy [40], and thus the parton density in the transverse nucleon area is about $1/\text{fm}^2$; hence the above estimate of τ_0 appears applicable. The number of partons in a nucleon increases with c.m.s. collision energy roughly as $s^{1/6}$ [40], so that the density at RHIC becomes about $2/\text{fm}^2$, at the LHC about $6/\text{fm}^2$. In Fig. 25, we show the initial energy densities for central $A-A$ collisions with $A = 200$; the range shown extends from the value based on $\tau_0 = 1$ fm to that obtained if we scale τ_0 accord to the mentioned parton densities, always with $w_h \simeq 0.5$ GeV. We note that in all cases the energy densities exceed the deconfinement value $\epsilon(T_c) \simeq 0.5 - 1.0$ GeV/ fm^3 . We also indicate which temperatures are expected to be accessible at the different facilities, using the results of Fig. 1.

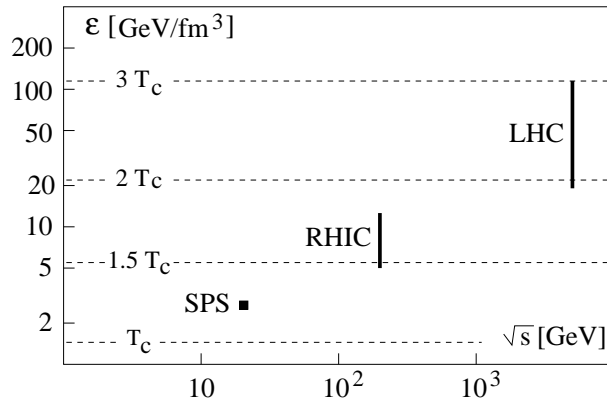


Figure 25: Energy density estimates vs. maximum collision energies, for different accelerators, compared to corresponding temperature

In the following sections, we shall try to show how one can probe deconfinement in nuclear collisions, based on the analysis of charmonium production; the extension to bottomonium is quite straightforward. First, the production of the probe must be understood when there is no bulk medium, so that we begin with charmonium production in elementary collisions. Next, one has to understand the modifications arising when the production occurs in a confined medium, for which $p-A$ collisions provide the experimental reference. With the probe thus prepared and gauged in confined matter, it can be applied in an environment in which there might be deconfinement.

5.2 Hadroproduction of Charmonia

The hadroproduction of charmonia occurs in three stages. The first stage is the production of a $c\bar{c}$ pair; because of the large quark mass, this process is well described by perturbative QCD (Fig. 26). A parton from the projectile interacts with one from the target; the (non-perturbative) parton distributions within the hadrons are determined empirically in other

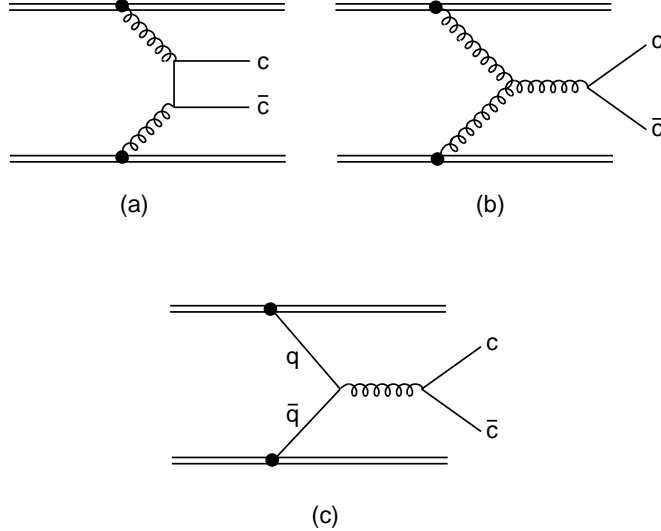


Figure 26: Lowest order diagrams for $c\bar{c}$ production in hadronic collisions, through gluon fusion (a,b) and quark-antiquark annihilation (c).

reactions, e.g. by deep inelastic lepton-hadron scattering. The produced $c\bar{c}$ pair is in general in a colour octet state. In the second stage, it neutralises its colour, leading to the third stage, physical resonances, such as J/ψ , χ_c or ψ' . Colour neutralisation occurs by interaction with the surrounding colour field; this and the corresponding resonance binding are presumably of non-perturbative nature.

On a fundamental theoretical level, colour neutralization is not yet fully understood. However, the colour evaporation model [41] provides a simple and experimentally well-supported phenomenological approach. In the evaporation process, the $c\bar{c}$ can either combine with light quarks to form open charm mesons (D and \bar{D}) or bind with each other to form a charmonium state. The basic quantity in this description is the total subthreshold charm cross section $S_{c\bar{c}}$, obtained by integrating the perturbative $c\bar{c}$ production cross section σ over the mass interval from $2m_c$ to $2m_D$. At high energy, the dominant part of $S_{c\bar{c}}$ comes from gluon fusion (Fig. 26a), so that we have

$$S_{c\bar{c}}(s) \simeq \int_{2m_c}^{2m_D} d\hat{s} \int dx_1 dx_2 g_p(x_1) g_t(x_2) \sigma(\hat{s}) \delta(\hat{s} - x_1 x_2 s), \quad (39)$$

with $g_p(x)$ and $g_t(x)$ denoting the gluon densities, x_1 and x_2 the fractional momenta of gluons from projectile and target, respectively; σ is the $gg \rightarrow c\bar{c}$ cross section. In pion-nucleon collisions, there are also significant quark-antiquark contributions (Fig. 26c), which become dominant at low energies. The basic statement of the colour evaporation model is that the production cross section of any charmonium state i is a fixed fraction of the subthreshold charm cross section,

$$\sigma_i(s) = f_i S_{c\bar{c}}(s), \quad (40)$$

where f_i is an energy-independent constant to be determined empirically. It follows that the energy dependence of the production cross section for any charmonium state

is predicted to be that of the perturbatively calculated sub-threshold charm cross section. As a further consequence, the production ratios of different charmonium states

$$\frac{\sigma_i(s)}{\sigma_j(s)} = \frac{f_i}{f_j} = \text{const.} \quad (41)$$

must be energy-independent. Both these predictions have been compared in detail to charmonium and bottomonium hadroproduction data over a wide range of energies [42]; they are found to be well supported, both in the energy dependence of the cross sections and in the constancy of the relative species abundances. Let us consider in more detail what this tells us about the hadronization of charm quarks.

We recall that the relative abundances of light hadrons produced in hadron-hadron and e^+e^- interactions follow the statistical pattern governed by phase space weights [43, 44]: the relative production rates are those predicted by an ideal resonance gas at the confinement/deconfinement transition temperature $T_c \simeq 175$ MeV. For two hadron species i and j that implies at all (high) collision energies

$$R_{i/j} \simeq \frac{d_i}{d_j} \left(\frac{m_i}{m_j} \right)^{3/2} \exp -\{(m_i - m_j)/T_c\} \quad (42)$$

for the ratio of the production rates, with d_i for the degeneracy (spin, isospin) and m_i for the mass of species i . For strange particles, the rates (42) overpredict the experimental data; this can, however, be accommodated by a common strangeness suppression factor $\gamma_s \simeq 0.5$, applied as γ_s^n if the produced hadron contains n strange quarks.

For the hadroproduction of charm, such a statistical description does not work, as seen in three typical instances:

- The total $c\bar{c}$ cross section increases with energy by about a factor ten between $\sqrt{s} = 20$ and 40 GeV, while the light hadron multiplicity only grows by about 20%. Hence the ratios for hadrons with and without charm are not energy-independent.
- From $p - p$ data one finds for J/ψ production a weight factor $f_{J/\psi} \simeq 2.5 \times 10^{-2}$ [42]. Since the subthreshold $c\bar{c}$ cross section is about half of the single D production cross section [45], this implies $R_{(J/\psi)/D} \simeq 10^{-2}$; the ideal resonance gas gives with $R_{(J/\psi)/D} \simeq 10^{-3}$ a prediction an order of magnitude smaller. Of the total charm production, more goes into the hidden charm sector than statistically allowed.
- For the production ratio of ψ' to J/ψ , which have the same charm quark infrastructure, one finds experimentally over a wide range of collision energies $R_{\psi'/(J/\psi)} \simeq 0.23$. This energy-independent ψ' to J/ψ ratio can be accounted for in terms of the charmonium masses and wave functions; it disagrees strongly with the statistical prediction, which gives with $R_{\psi'/(J/\psi)} \simeq 0.045$ a very much smaller value. The same holds true for the other measured charmonium states, as seen in Table 4, where we list experimental results obtained in 300 GeV/c π and proton interactions [46]. All ratios are given relative to directly produced (1S) J/ψ states.

While the first two points could be accommodated by an energy-dependent ‘charm enhancement’ factor, the last rules even this out. In the presently available collision energy range, charm production in elementary collisions thus does not seem to be of statistical

nature. It appears to be determined by parton dynamics at an early stage, rather than by the phase space size at the confinement temperature.

ratio	$\psi'/(J/\psi)$	$\chi_{c1}/(J/\psi)$	$\chi_{c2}/(J/\psi)$
experimental	0.23	1.06	1.50
statistical	0.045	0.113	0.148

Table 4: Charmonium production ratios vs. statistical predictions

Although the colour evaporation model provides a viable phenomenological description of the hadroproduction of quarkonia, leading to correct quantitative predictions up to the highest energies under consideration, it cannot predict the fractions f_i of the hidden charm cross sections, and it can even less describe the space-time evolution of colour neutralization. For charmonium production in p-A and A-B collisions, the latter is crucial, however, and hence a more detailed description of colour neutralization is needed.

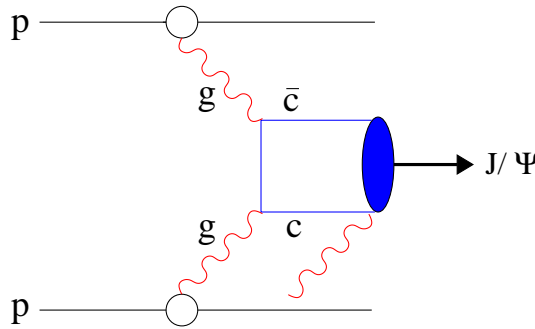


Figure 27: The evolution of J/ψ production

The colour octet model [47] proposes that the colour octet $c\bar{c}$ combines with a soft collinear gluon to form a colour singlet ($c\bar{c}-g$) state. After a rather short relaxation time τ_8 , this pre-resonant ($c\bar{c}-g$) state turns into the physical $c\bar{c}$ mode by absorbing the accompanying gluon, with similar formation processes for χ_c and ψ' production. The colour octet model encounters difficulties if the collinear gluons are treated perturbatively, illustrating once more that colour neutralization seems to require non-perturbative elements [48]. However, it does provide a conceptual basis for the evolution of the formation process (see Fig. 27). The colour neutralization time τ_8 of the pre-resonant state can be estimated [49]; it is essentially determined by the lowest momentum possible for confined gluons, $\tau_8 \simeq (2m_c l)^{1/2} \simeq 0.25$ fm. The resulting scales in J/ψ formation are illustrated in Fig. 28. The formation time for the actual physical ground state J/ψ is presumably somewhat larger than τ_8 ; although $r_{J/\psi} \simeq \tau_8$, the heavy c quarks do not move with the velocity of light. For the larger higher excited states, the formation times will then be correspondingly larger.

There is one further important feature to be noted for J/ψ hadroproduction. The J/ψ 's

0.05 fm	0.25 fm
hard	pre-resonance resonance
$\tau_{c\bar{c}} = 1/2m_c$	$\tau_8 = 1/\sqrt{2}m_c \Lambda_{\text{qcd}}$

Figure 28: Scales of J/ψ production

actually measured in hadron-hadron collisions have three distinct origins: about 60 % are directly produced 1S charmonium states, while about 30 % come from the decay $\chi_c(1P) \rightarrow J/\psi + \text{anything}$, and the remaining 10 % from $\psi'(2S) \rightarrow J/\psi + \text{anything}$ [50]. Such feed-down also occurs in Υ production [51]. In all cases, the decay widths of the involved higher excited states are extremely small (less than one MeV), so that their lifetimes are very long. The presence of any medium in nuclear collisions would therefore affect these excited states themselves, and not their decay products.

5.3 Charmonium Production in $p - A$ Collisions

We have seen that in the use of charmonia to study nuclear collisions, the creation of the medium and the production of the probe lead to two distinct formation scales, τ_0 and τ_8 . In $p - A$ collisions, the presence of normal nuclear matter can affect charmonium production. Here there is no formation time for the medium, so that such collisions provide a tool to probe charmonium production, evolution and absorption in confined matter.

Nuclear effects can arise in all the evolution stages of J/ψ production, and a number of different phenomena have been studied in considerable detail.

- The presence of other nucleons in the nucleus can modify the initial state parton distribution functions, which enter in the perturbative $c\bar{c}$ production process illustrated in Fig. 26. This can lead to a decrease (*shadowing*) or to an increase (*antishadowing*) of the production rate.
- Once it is produced, the $c\bar{c}$ pair can suffer *absorption* in the pre-resonance as well as in the resonance stage, caused by the successive interactions with the target nucleons.
- The extent of this absorption can moreover be modified through *coherence* effects for the interactions on different nucleons, which can lead to partial cancellation (Landau-Pomeranchuk-Migdal effect).

In all cases, the crucial quantity is the momentum of the charmonium state as measured in the nuclear target rest frame.

Since we eventually want to probe the effect which the ‘secondary’ medium *produced* by nucleus-nucleus collisions has on charmonium production, it is of course essential to account correctly for any effects of the nuclear medium initially present. Let us therefore first summarize the main features observed for charmonium production in $p - A$ collision experiments [52].

- At fixed collision energy, quarkonium production rates per target nucleon decrease with increasing A .
- The production rates decrease for increasing J/ψ momentum as measured in the nuclear target rest frame.
- The nuclear reduction at $p - N$ mid-rapidity appears to become weaker with increasing collision energy.
- For fixed collision energy, mass number A and J/ψ rapidity, the reduction appears to increase with the centrality of the collision.
- At sufficiently high momentum in the target rest frame, the different charmonium states appear to suffer the same amount of reduction, while at lower energy, the ψ' is affected more than the J/ψ .

At present, there does not seem to exist a theoretical scenario able to account quantitatively for all these observations. In fact, so far not even a common scaling variable for the different effects has been found. Shadowing would suggest scaling in the fractional target parton momentum x_2 , while absorption of the pre-resonance state would point to the fractional beam momentum x_F . Neither is in good accord with the data. For a further discussion, we therefore refer to recent reviews [52, 53] and concentrate here on obtaining some operational methods to specify nuclear effects in $p - A$ collisions in a way that can be extended to $A - B$ collisions. This, incidentally, illustrates the crucial importance of having $p - A$ data in order to arrive at an interpretation of $A - A$ results; for future LHC experiments, where parton saturation may play a crucial role, this is even more so the case.

Consider the production of a charmonium state in a $p - A$ collision [54]. If the initial $c\bar{c}$ production process occurs at a random point inside the nucleus, the evolving charmonium state will on the average traverse a path of length $L_A = 3R_A/4$ through nuclear matter. We have to know in what stage of its evolution the charmonium will be along this path. The distance travelled by the charmonium is, in the rest frame of the nucleus, given by

$$d = \tau \left(\frac{P_A}{M} \right) \quad (43)$$

where P_A is the charmonium momentum in the nuclear rest frame, M the mass and τ the proper age of the charmonium, i.e., its lifetime in its own rest frame. For simplicity, we consider for the moment only charmonia produced at rest in the center of mass of a proton-nucleon collision ($x_F = 0$), where most of the data are taken. Then we have

$$P_A \simeq \frac{M}{2m} \sqrt{s}, \quad (44)$$

with m for the nucleon mass and \sqrt{s} for the proton-nucleon c.m.s. collision energy. In Table 5, we show as illustration the resulting values for the charmonium momenta P_A in the nuclear rest frame at different collision energies; FNAL refers to the energy of the fixed target program. We also give the corresponding colour neutralization path lengths

$d_8 = d(\tau = \tau_8)$. Note that these are the values for $x_F = 0$; P_A and d_8 depend quite sensitively on x_F .

accelerator	\sqrt{s} [GeV]	P_A [GeV]	d_8 [fm]
SPS	17	29	2
SPS	29	48	4
FNAL, HERA B	40	66	5
RHIC	200	330	26
LHC	5500	9000	730

Table 5: Charmonium formation parameters at $x_F = 0$ for different collision energies

We now follow the charmonium in time along its path through the nucleus. For times shorter than the colour neutralization time τ_8 , $\tau < \tau_8$, the nucleus is traversed by a pre-resonance state, which can be dissociated through interaction with nuclear matter, with a dissociation cross section σ_{diss} . For $\tau > \tau_8$, the physical resonance passes through the remaining nuclear medium. From Table 5 we note that for RHIC and LHC, the colour neutralization point lies well outside any nucleus, so that there the nuclear medium only sees the pre-resonance state. For FNAL and HERA B, d_8 is approximately equal to the size of the largest nuclei, so that here as well only pre-resonance effects should play a role. Since up to times τ_8 the different charmonium states are indistinguishable, absorption effects for $\sqrt{s} > 40$ GeV (at $x_F = 0$) should be the same for all states. At the SPS, both pre-resonance and resonance absorption can come into play, so that the effect should be stronger for the ψ' than for the J/ψ . Here it should be noted, however, that in both cases, the expansion of the $c\bar{c}$ occurs with less than the speed of light, so that at $\tau = \tau_8$ the colour singlet is not yet of physical size.

Let us now quantify these considerations [55]. According to the Glauber formalism of nuclear scattering theory, a $c\bar{c}$ pair formed at point z_0 in a target nucleus A has a survival probability

$$S_i^A = \int d^2b dz \rho_A(b, z) \exp \left\{ -(A-1) \int_{z_0}^{\infty} dz' \rho_A(b, z') \sigma_{\text{diss}}^i \right\}, \quad (45)$$

where the integration covers the path, at impact parameter b , remaining from z_0 out of the nucleus, and where σ_{diss}^i describes the overall ‘‘absorption’’ effect on the observed charmonium state i along the path. The result is then averaged over impact parameter and path lengths. The traversed medium of nucleus A is parametrized through a Woods-Saxon density distribution $\rho_A(z)$, and by comparing S_i to data for different targets A , the effective dissociation cross section can be obtained for the J/ψ and ψ' absorption in nuclear matter. The effect of the charmonium passage through the nucleus will arise from

a superposition of the different stages; but if part of the passage is carried out as physical resonance, higher excited states should lead to larger absorption cross-sections than the much smaller ground state J/ψ . In accord with this, the most recent SPS analysis, based on $p-A$ collisions with Be , Al , Cu , W and Pb targets, gives [56]

$$\sigma_{J/\psi} = 4.18 \pm 0.35 \text{ mb} \quad (46)$$

for the J/ψ , and

$$\sigma_{\psi'} = 7.3 \pm 1.6 \text{ mb} \quad (47)$$

for the ψ' as nuclear absorption cross sections at $\sqrt{s} \simeq 29 \text{ GeV}$.

Data from the SPS were taken for a number of different nuclear targets, but so far no information on the centrality-dependence of the results has been given. In contrast, RHIC experiments have provided only data for $d-Au$ collisions, but as function of centrality and for three different rapidity ranges [57]. In the central rapidity range $|y| \leq 0.35$, the data is obtained from e^+e^- measurements, in the larger rapidity intervals $1.2 \leq y \leq 2.2$ and $-2.2 \leq y \leq -1.2$ through forward and backward $\mu^+\mu^-$ detection. The results are shown in Fig. 29, where

$$R_{d-Au}(y) = \frac{(d\sigma/dy)_{d-Au}}{N_{coll} (d\sigma/dy)_{p-p}} \quad (48)$$

measures the nuclear modification in the given y range, relative to the corresponding $p-p$ cross section scaled by the number N_{coll} of binary nucleon-nucleon collisions. This number is obtained from the measured number of participant nucleons through a Glauber analysis and is also used to parametrize the centrality dependence.

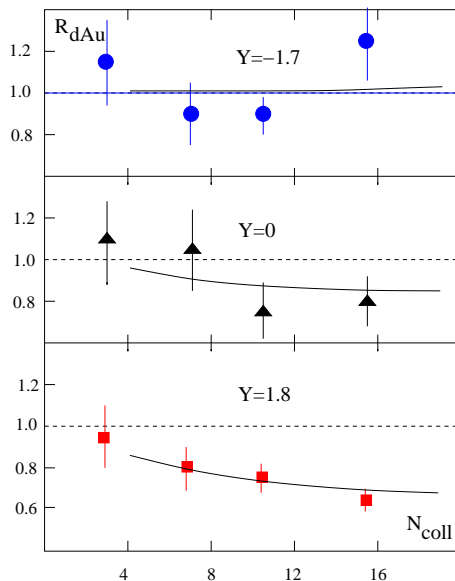


Figure 29: J/ψ production in $d-Au$ collisions at RHIC [57]

So far, within the rather limited statistics available, it is not easy to quantify these RHIC results enough to obtain a reasonable estimate of normal nuclear effects. As first attempt, we adopt a similar parametrization as used for SPS results and apply the well-known simplified form of eq. (45),

$$S \simeq \exp\{-n_0\sigma_{diss}L\}, \quad (49)$$

where L denotes the path of the $c\bar{c}$ in the nuclear medium. Glauber analysis [58] provides the relation between impact parameter b and the number of collisions N_{coll} , and simple geometry gives $L^2 = R_A^2 - b^2$ in terms of b and the nuclear radius R_A . A fit of Eq. (49) to the data of Fig. 29 gives¹

$$\begin{aligned}\sigma_{diss}(y = 1.8) &= 3.1 \pm 0.2 \text{ mb} \\ \sigma_{diss}(y = 0) &= 1.2 \pm 0.4 \text{ mb} \\ \sigma_{diss}(y = -1.7) &= -0.1 \pm 0.2 \text{ mb}\end{aligned}\tag{50}$$

for the corresponding J/ψ dissociation cross sections; for $y = -1.7$, there thus are essentially no nuclear modifications. We note that here, as for the SPS case, these cross sections are just a global way to account for whatever nuclear effects can arise. A more detailed analysis based on shadowing and absorption is given in [59].

5.4 Charmonium Production in Nuclear Collisions

The basic assumption in the attempt to create deconfined matter through nuclear collisions is that the excited vacuum left after the passage of the colliding nuclei forms a thermal medium. This picture is schematically illustrated in Fig. 30. A charmonium state produced in such a collision will in its early stages always be subject to the possible effects of the nuclear medium, just as it is in $p-A$ collisions. Knowing the $p-A$ behaviour at the corresponding energy is thus a necessary baseline for probing the additional effects of the produced medium.

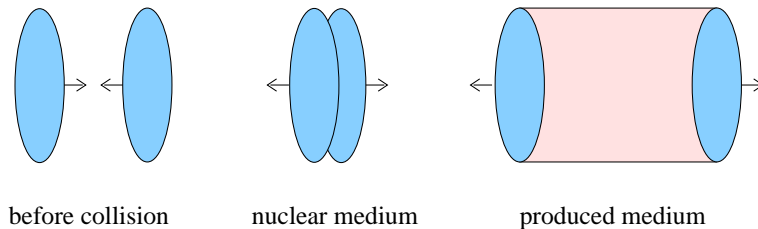


Figure 30: Collision stages

The Glauber formalism used above to calculate the survival probability of an evolving charmonium state in a $p-A$ collision now has to be extended to $A-B$ interactions [55]. The survival probability at impact parameter b now becomes

$$\begin{aligned}S_i^{AB}(b) &= \int d^2s dz dz' \rho_A(s, z) \rho_B(b-s, z') \times \\ &\exp \left\{ -(A-1) \int_{z_0^A}^{\infty} dz_A \rho_A(s, z_A) \sigma_i - (B-1) \int_{z_0^B}^{\infty} dz_B \rho_B(b-s, z_B) \sigma_i \right\},\end{aligned}\tag{51}$$

as extension of Eq. (45). Here z_0^A specifies the formation point of the $c\bar{c}g$ within nucleus A , z_0^B its position in B . With the dissociation cross sections σ_{diss}^i determined in $p-A$

¹In the fit, we neglect the most peripheral point at N_{coll} , which corresponds to $b > R_{Au}$ and is thus due to nuclear surface rather than medium effects.

collisions, Eqs. (46/47), the ‘normal’ survival probability, i.e., that due to only the nuclear medium, is fully specified.

Since experiments cannot directly measure the impact parameter b , we have to specify how Eq. (51) can be applied to data. The Glauber formalism allows us to calculate the number $N_w^{AB}(b)$ of participant (‘wounded’) nucleons for a given collision as function of centrality. In $A-A$ collisions, the number of unaffected ‘spectator’ nucleons $N_s^A(b)$ can be determined directly through the use of a zero-degree calorimeter, and hence $N_w^{AA}(b) = 2A - 2N_s^A(b)$ is accessible experimentally. For asymmetric AB collisions, the situation is somewhat more complex.

At RHIC energy, we make again use of the simplified form (49). The geometry connecting the impact parameter b and path length L in $p-Au$ and $Au-Au$ collisions is illustrated in Fig. 31; the relation between b and N_{part} is again given by a Glauber analysis [60]. The resulting survival probability is

$$S_i^{AA}(y, N_w) = \frac{R_{AA}(y, N_w)}{\exp\{-n_0[\sigma_{\text{diss}}(y) + \sigma_{\text{diss}}(-y)]L\}}, \quad (52)$$

corresponding to the fact that, for $y \neq 0$, the charmonium state passes one nucleus at rapidity y and the other at rapidity $-y$.

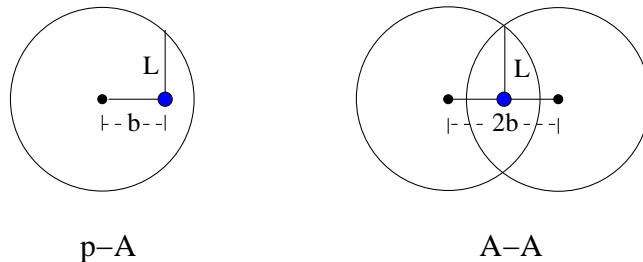


Figure 31: Impact parameter relation between $p-A$ and $A-A$ collisions

Eqs. (51) and (52) specify the suppression pattern for charmonium states as predicted from normal nuclear effects. To use quarkonia as probes for the produced medium, we now have to study how the behaviour observed in $A-A$ collisions differs from this predicted pattern.

Several possible and quite different effects have been considered as consequences of the produced medium on quarkonium production. To be specific, we again consider the charmonium case for illustration.

- **Suppression by comover collisions:** A charmonium state produced in a primary nucleon-nucleon collision can be dissociated through interactions with the constituents of any medium subsequently formed in the collision. Such dissociation could occur in a confined [61] as well as in a deconfined medium [21].
- **Suppression by colour screening:** If the produced medium is a hot QGP, it will dissociate by colour screening the charmonium states produced in primary nucleon-nucleon collisions. Due to the rareness of thermal charm quarks in the medium, the separated c and \bar{c} combine at hadronization with light quarks to form open charm mesons [3].

- Enhancement by recombination: In the hadronization of the QGP, charmonium formation can occur by binding of a c with a \bar{c} from different nucleon-nucleon collisions, as well as from the same. If the total number of available $c\bar{c}$ pairs considerably exceeds their thermal abundance, statistical recombination enhances hidden relative to open charm production, as compared to hadron-hadron collisions [62].

In addition, the partonic initial state of the colliding nuclei, which leads to the formation of the produced medium and to that of charmonium states, will change its nature with increasing A and/or \sqrt{s} ; eventually, parton percolation (colour glass formation) can lead to a very different medium, with possible effects on production and binding of charmonia [63].

Is it possible for experiment to distinguish between these different scenarios? Before turning to the experimental situation, we want to discuss in some more detail the salient features of each approach.

Suppression by Comover Collisions

If the charmonium state moves in a random scattering pattern through the produced medium, its survival rate is approximately given by

$$S_i = \exp\{-\sigma_i n \tau_0 \ln[n/n_f]\} \quad (53)$$

with σ_i denoting the dissociation cross section, n the initial density of the medium after a formation time τ_0 , and n_f the ‘freeze-out’ density, at which the interactions stop.

Since the cross section for J/ψ break-up through gluon collisions is large [21] and the gluon density high, there will be significant charmonium suppression in a deconfined medium, even if this is not thermalized. In an equilibrium QGP, this dissociation is presumably accounted for by colour screening, provided the effect of the medium on the width of the surviving states is also calculated.

Charmonium dissociation by interaction with hadronic comovers has received considerable attention in the past [61]. However, if one restricts the possible densities to values appropriate to hadronic matter ($n_h \lesssim 0.5 \text{ fm}^{-3}$) and the cross sections to those obtained in chapter 5, the effect of hadron dissociation is negligible. Even a cross section increase to the high energy limit still leads to less than 10% effects. More recent analyses [64] thus conclude that a hadronic medium will not result in significant suppression.

In Fig. 32 we illustrate schematically the overall behaviour expected for J/ψ dissociation through comover collisions, assuming that beyond a deconfinement threshold, the comover density increases with energy density in a monotonic fashion, with little or no prior suppression in the hadronic regime.

Suppression by Colour Screening

The theoretical basis of this effect has been considered in detail in chapter 5; the colour field between the heavy quarks becomes modified due to the presence of a medium of unbound colour charges. The results obtained for this effect in statistical QCD are as such model-independent, once all calculational constraints are removed. What is speculative

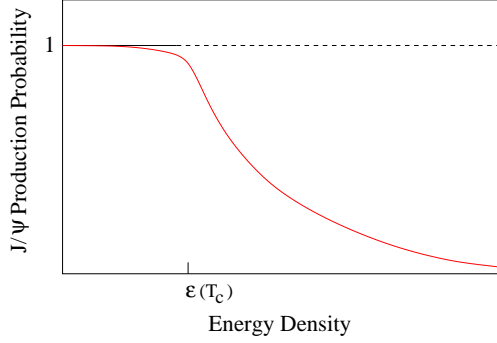


Figure 32: J/ψ suppression by comover collisions

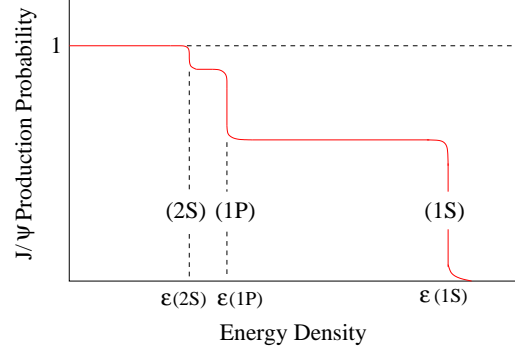


Figure 33: Sequential J/ψ suppression by colour screening

and model-dependent is its application to nuclear collisions: these do not necessarily produce the medium studied in thermal QCD, and the different evolution stages in nuclear collisions can introduce factors not present in the study of equilibrium thermodynamics, such as the oversaturation of $c\bar{c}$ pairs just mentioned.

If the medium produced in high energy nuclear collisions is indeed the quark-gluon plasma of statistical QCD, and if charmonium production can be treated as a distinct process within such an environment, then the effect of colour screening seems clear. The partition of the $c\bar{c}$ pairs produced in nucleon-nucleon collisions into hidden and open charm is non-statistical, favouring the hidden charm sector because of dynamical binding effects. Colour screening destroys these and hence moves the partition more and more towards a statistical distribution, thus suppressing charmonium production rates relative to those observed in elementary interactions.

A crucial feature of J/ψ suppression by deconfinement is its sequential nature [65, 66]. In the feed-down production of J/ψ , the produced medium affects the intermediate excited states, so that with increasing temperature or energy density, first the J/ψ 's originating from ψ' decay and then those from χ_c decay should be dissociated. Only considerably higher temperatures would be able to remove the directly produced J/ψ 's. Such a step-wise onset of suppression, with specified threshold temperatures, is perhaps the most characteristic feature predicted for charmonium as well as bottomonium production in nuclear collisions. It is illustrated schematically in Fig. 33, where we have defined the J/ψ production probability to be unity if the production rate suffers only the calculated nuclear suppression.

Enhancement through Recombination

In charmonium hadroproduction, J/ψ 's are formed because some of the $c\bar{c}$ pairs produced in a given collision form a corresponding bound state. In a collective medium formed through superposition of many nucleon-nucleon (NN) collisions, such as a quark-gluon plasma, a c from one NN collision can in principle also bind with a \bar{c} from another NN collision. This 'exogamous' charmonium formation can lead to enhanced J/ψ production, provided the overall charm density of the medium at hadronization is sufficiently high and provided the binding probability between charm quarks from different sources is

large enough.

The production of $c\bar{c}$ pairs in primary collisions is a hard process and thus grows in $A - A$ interactions with the number of nucleon-nucleon collisions; in contrast, the multiplicity of light hadrons grows roughly as the number of participant nucleons. Hence the relative abundance of charm to non-charm quarks will be higher in $A - A$ than in $p - p$ collisions. Moreover, the $c\bar{c}$ production cross section increases faster with energy than that for light hadron production. The two effects together imply that in the medium produced in energetic $A - A$ collisions, the ratio of charm to non-charm quarks is initially much higher than in a equilibrated QGP. If this oversaturation of charm is preserved in the thermalization process, the combination of random c and \bar{c} quarks from different primary nucleon-nucleon interactions becomes more and more likely with increasing energy.

Whether or not such an enhancement becomes significant depends on two factors. On one hand, the initial charm oversaturation must be preserved, so that the total charm abundance is non-thermal. On the other hand, it is necessary that the ‘recombination’ of the pairs into charmonia is sufficiently strong. Here it is generally assumed that the final hadronization occurs according to the available phase space. Thus the number of statistically recombined J/ψ ’s has the form $N_{J/\psi} \sim N_{c\bar{c}}^2/N_h$, growing quadratically in the number of produced $c\bar{c}$ pairs; here N_h denotes the number of light hadrons (or quarks). This implies that the hidden to open charm ratio, e.g., $N_{J/\psi}/N_D \sim N_{c\bar{c}}/N_h$, increases with energy, in contrast to the energy independent form obtained for a fully equilibrated QGP, or to the decrease predicted by colour screening.

Several studies of this effect have led to different noticeable enhancement factors [67], in the strongest form even predicting an overall enhancement of J/ψ production in $A - A$ collisions relative to $p - p$ results scaled by binary collisions. A crucial prediction of the approach is the *increase* of the enhancement with centrality, as shown in Fig. 34, because of the corresponding increase in the number of collisions and hence of the number of $c\bar{c}$ pairs.

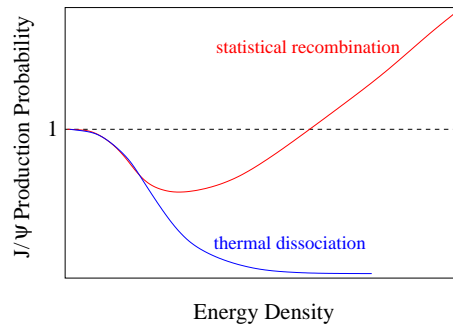


Figure 34: J/ψ enhancement by recombination

Initial State Suppression

For two colliding nuclei at large enough A or \sqrt{s} , the density of partons in the transverse plane becomes so large (see Fig. 24) that the partons percolate, producing an interconnected network. If the resolution scale of the partons in this network is sufficient to resolve charmonia, it could also dissociate them. This scenario is in many ways similar

to suppression by colour screening, but it is on the whole more model-dependent. Given the average transverse size of the partons in terms of the resolution scale of the parton distribution function, it is possible to calculate the percolation point; but its effect on the different charmonium states is not *a priori* evident and can only be addressed in models [63, 68].

In other words, the relation between the onset of charmonium dissociation and the percolation point remains so far of phenomenological nature. In contrast to thermal QCD, it does not seem possible here to evaluate dissociation points from basic theory. One promising approach might be the study of quarkonium dissociation in the strong classical colour fields created in the percolating medium through the onset of colour glass formation.

6. Experimental Results from Nucleus-Nucleus Collisions

Over the past twenty years, great experimental efforts have produced a wealth of data on charmonium production in nucleus-nucleus collisions. The pioneering work of the NA38 and NA50 collaborations at the SPS led to the second generation experiment NA60, which is just now announcing its first results. At the same time, RHIC is providing us with a first look at how things change when the collision energy is increased by a factor ten. It is certainly an exciting time; but although the results may give some indications, more information is necessary in order to reach final conclusions. So let us try to summarize what we know today and then try to point out what that could mean and what more is needed before we can be sure.

6.1 SPS Results

Extensive data was taken for $S-U$ collisions (NA38) at $\sqrt{s} = 19.4$ GeV and for $Pb-Pb$ (NA50) collisions at $\sqrt{s} = 17.3$ GeV, for J/ψ [69, 70] and for ψ' production [71], as well as the mentioned reference data for $p-A$ interactions. The main aspects of the NA38/NA50 results are shown in Fig. 35. Here the charmonium production rates are measured relative to Drell-Yan pair production in the same collision configuration, and the resulting ratio is then normalized to the value expected when normal nuclear absorption is taken into account, with the cross sections of eqs. (46/47). The centrality is experimentally determined either by a zero degree calorimeter, which measures the overall spectator energy (E_{ZDC}) and thus leads directly to the number of participant nucleons, or through the transverse energy (E_T) or multiplicity of the produced hadrons. The results are shown as function of centrality as given by the average length L of nuclear matter traversed, which can be determined through a Glauber analysis of either E_{ZDC} or E_T data.

In summary, we note the following behaviour:

- The rates for J/ψ and ψ' production in $p-A$ collisions are correctly accounted for by normal nuclear absorption.
- J/ψ production in $S-U$ collisions at $\sqrt{s} = 20$ GeV is compatible with normal nuclear absorption. ψ' production in the same $S-U$ collisions, however, shows a further reduction. This is the first instance of an ‘anomalous’ suppression, decreasing the normal rate by up to a factor five in the most central collisions.

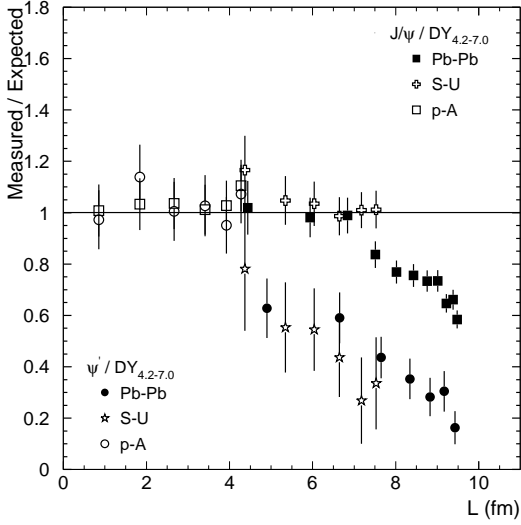


Figure 35: J/ψ and ψ' production from NA38/NA50 [69]

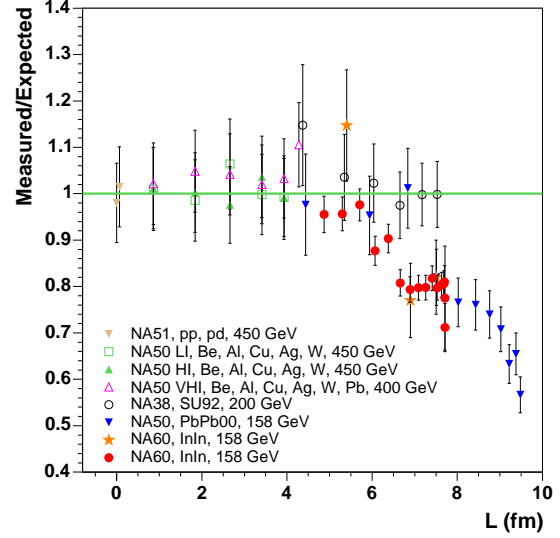


Figure 36: J/ψ production from NA38/NA50/NA51/NA60 [70]

- J/ψ production in $Pb-Pb$ collisions at $\sqrt{s} \simeq 17$ GeV as function of centrality shows an onset of anomalous suppression. While peripheral results again agree with extrapolated $p-A$ results, beyond some centrality there is an additional reduction by some 20 - 40 %. The anomalous ψ' suppression in $Pb-Pb$ interactions starts for more peripheral collisions than that for J/ψ , and as function of the available medium it is compatible to the $S-U$ results.

The onset of anomalous J/ψ suppression in $Pb-Pb$ collisions and its absence in $S-U$ interactions suggested studying a lighter $A-A$ combination, to obtain further information about this phenomenon. The NA60 collaboration has now presented first results on J/ψ production in $In-In$ collisions [70]; they are shown in Fig. 36, together with the other J/ψ data taken at the SPS.

- In $In-In$ collisions there is again an onset of anomalous J/ψ suppression, which here, however, appears to occur at a centrality at which the corresponding $S-U$ data do not show any such effect. The $Pb-Pb$ data is within errors compatible with an earlier as well as a later onset position.

Finally we note that also the transverse momentum behaviour of J/ψ production in $p-A$ and $A-A$ collisions was studied at the SPS [72].

- As shown in Fig. 37, the average (squared) J/ψ transverse momentum increases with the amount of nuclear matter. A detailed view of the $Pb-Pb$ results in Fig. 38 suggests a reduced broadening rate for more central collisions.

6.2 RHIC Results

In the past months, the PHENIX collaboration at RHIC has presented J/ψ production results at $\sqrt{s} = 200$ GeV for $d-Au$, $Au-Au$ and $Cu-Cu$ collisions [73]. We should note that the increase of a factor ten in collision energy corresponds to an increase by a

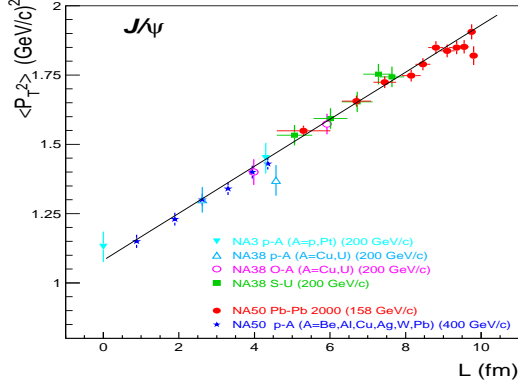


Figure 37: Transverse momentum behaviour of J/ψ production [72]

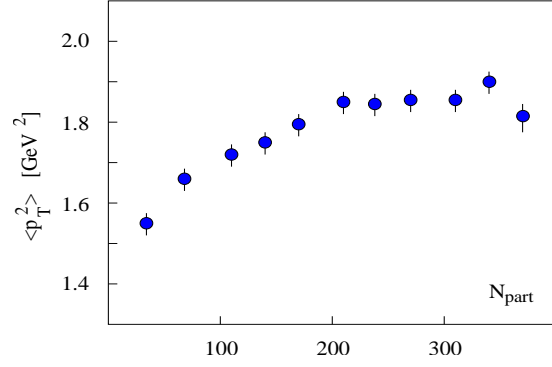


Figure 38: J/ψ transverse momentum behaviour in $Pb - Pb$ collisions [72]

factor two to four in energy density, depending on the value of τ_0 , so that the new data smoothly extend the regime studied so far. The data are generally presented in the form of a nuclear modification factor R_{AA} , giving the J/ψ production rate in $Au-Au$ collisions relative to the $p-p$ rate scaled up by the number of binary collisions.

The results for $Au-Au$ collisions² at $\sqrt{s} = 200$ GeV are given for two rapidity ranges, $|y| \leq 0.35$ and $|y| \in [1.2, 2.2]$, as was the case for the reference $d-Au$ collisions (Fig. 29). The resulting rates R_{AA} are shown in Fig. 39.

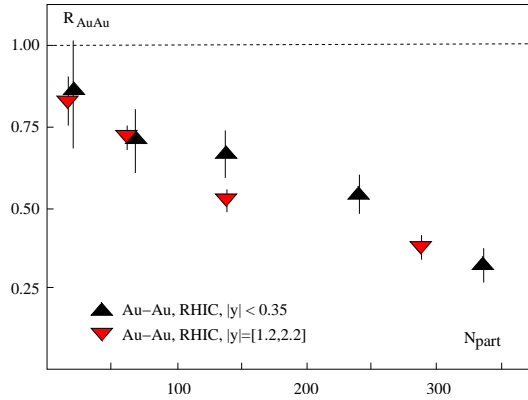


Figure 39: J/ψ production rates at RHIC [73]

The corresponding survival probabilities can now be determined by eq. (52), making use of the nuclear medium modification through the simplified Glauber form (49). Since the resulting cross sections are so far known with very limited accuracy, we do not include the additional error arising from R_{dAu} . In Fig. 40, we show the J/ψ survival probability in $Au-Au$ collisions for the two rapidity intervals, as function of the number of participants N_{part} . The suppression is seen to increase with centrality, up to a survival rate of 40 - 60% remaining for the most central $Au-Au$ interactions.

²We shall not consider the results of the $Cu-Cu$ interactions here, since at present we do not have access to the corresponding Glauber studies needed for comparison.

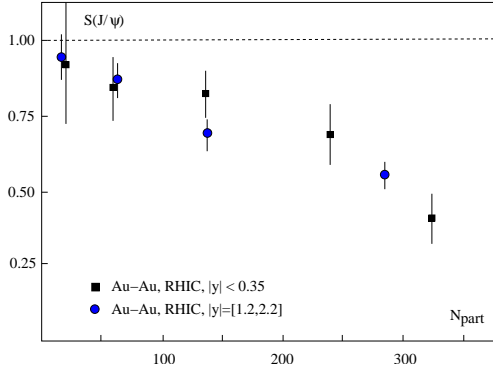


Figure 40: J/ψ survival probability at RHIC

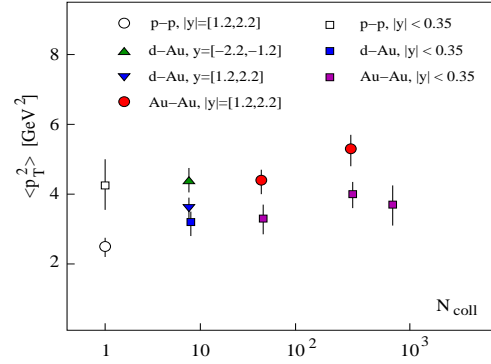


Figure 41: J/ψ transverse momentum behaviour at RHIC [73, 74]

Preliminary RHIC data on the transverse momentum behaviour of J/ψ production have also been presented [74]. As seen in Fig. 41, the muon arm results are similar to those obtained at the SPS, with increasing broadening from $p-p$ to $d-Au$ and on to $Au-Au$ as function of centrality. The e^+e^- data have so far very limited statistics and, in particular, do not (yet?) show a broadening when going from $p-p$ to $d-Au$.

6.3 What does it all mean?

High energy nuclear collision data thus provide a considerable amount of information on the in-medium behaviour of charmonium production. We recall that the *raison d'être* for the experimental programme was to study in the laboratory the deconfinement transition and the new deconfined state of matter predicted by statistical QCD. The crucial question in the present context is thus whether the pattern of charmonium suppression observed in heavy ion studies is in accord with that calculated in finite temperature lattice QCD. Here we should keep in mind that it is not *a priori* obvious that the medium produced in nuclear collisions is in fact the equilibrium QGP studied in statistical QCD. A quantitative relation between the charmonium suppression features in nuclear collisions and those calculated in lattice QCD would thus provide excellent support for QGP production. So where are we now? Does a combination of all the different aspects lead to some first conclusions? In this section, we want to address several issues that come up if we try to find a coherent interpretation.

We begin by recalling that if we want to compare data from different nuclear collisions and from different collision energies, we have to define some more or less ‘universal’ scale variable. We had shown SPS results as function of the effective path length L through nuclear matter, since much of the data was presented that way. From an experimental point of view, E_{ZDC} data gives the number of participants as the most directly measurable quantity, while from a theoretical point of view, density variables, such as participant density, energy density or parton density, are conceptually preferable. To compare different $A-B$ configurations at the same energy, the participant density n_{part} is still meaningful, but for different $A-B$ at different collision energies, one has to resort to energy or parton densities in order to accommodate the resulting modifications.

The first question that arises by looking at SPS results concerns the onset of anomalous

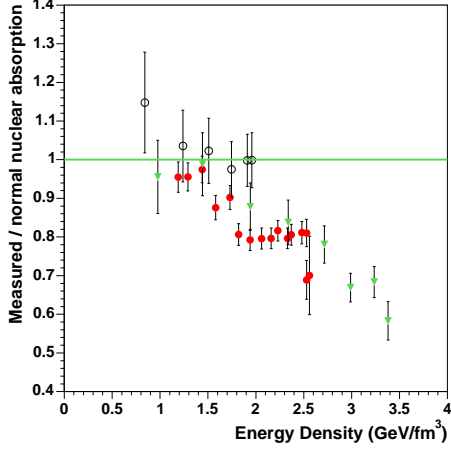


Figure 42: J/ψ production in $In-In$, $Pb-Pb$ collisions (E_{ZDC} data) and in $S-U$ collisions (E_T data) [70]

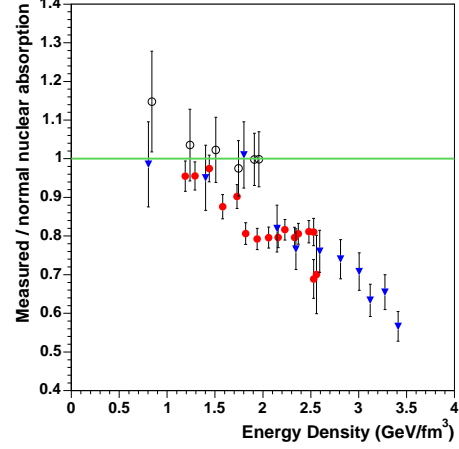


Figure 43: J/ψ production in $Pb-Pb$, $S-U$ collisions (E_T data) and in $In-In$ collisions (E_{ZDC} data) [70]

J/ψ suppression in $S-U$, $Pb-Pb$ and $In-In$ collisions. Do the data as shown in Fig. 36 imply different onsets in the different reactions? In Figs. 42 and 43 we see that the discrepancy between $S-U$ and $In-In$ remains, though less pronounced, when we determine the centrality through the energy density. We also note, however, that different experimental methods of determining the centrality can lead to slight differences. The onset of anomalous suppression in the $Pb-Pb$ data agrees very well with that found in the $In-In$ data when both are shown in terms of the E_{ZDC} determined centrality (Fig. 42), while an apparently later $Pb-Pb$ onset, in accord with the $S-U$ behaviour, is found for an E_T -based analysis (Fig. 43). Finally we also note that a 10% shift of the $S-U$ normalization would remove all differences. Further study here would thus seem very appropriate, with the aim of comparing only data in which the centrality determination is carried out in the same way (ideally, E_{ZDC} determined centrality) for different collision configurations and for both J/ψ and ψ' .

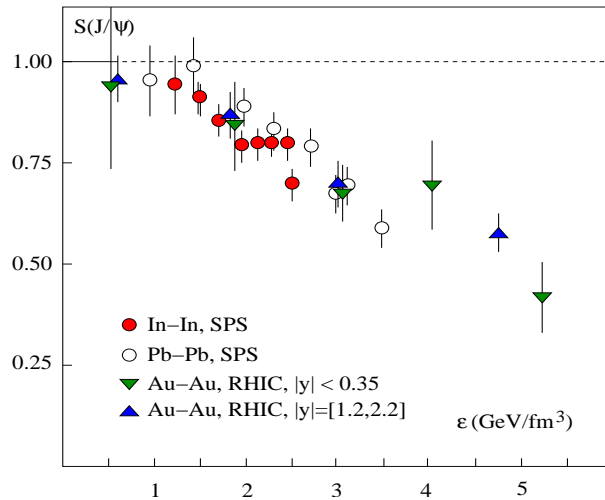


Figure 44: J/ψ suppression as function of energy density

In Fig. 44, we show the J/ψ survival probability $S_{J/\psi}$ for a combination of SPS and RHIC data as function of the energy density, with all data determined through E_{ZDC} measurements. For the RHIC data, the energy density values for the different centralities are obtained by a Glauber analysis based directly on the PHENIX data, with $\tau_0 = 1$ fm [75].

The suppression pattern shown in Fig. 44 is fairly consistent with that obtained in chapter 4 from finite temperature lattice QCD. We had found there a suppression of χ_c and ψ' just above T_c , which implies around $\epsilon \simeq 1$ GeV/fm³, while the $J/\psi(1S)$ should survive up to $\epsilon \simeq 10$ GeV/fm³ or more. For J/ψ production in nuclear collisions, this means a suppression of the 40% coming from χ_c and ψ' decay starting around 1 GeV/fm³, while the 60% directly produced J/ψ remain unaffected until much higher ϵ . The onset of the anomalous suppression in Fig. 44 occurs indeed at the expected energy density, and the J/ψ survival probability converges towards some 50 - 60%. Before considering the possibility of a next suppression onset at large ϵ , we should recall that the energy density values for the RHIC data were obtained with a formation time $\tau_0 = 1$ fm. As mentioned, τ_0 could well be smaller (parton densities suggest $\tau_0 = 0.5$ fm), which would move the RHIC points to correspondingly higher ϵ . However, given the present statistics, an interpretation of the large ϵ behaviour as onset would in any case seem premature.

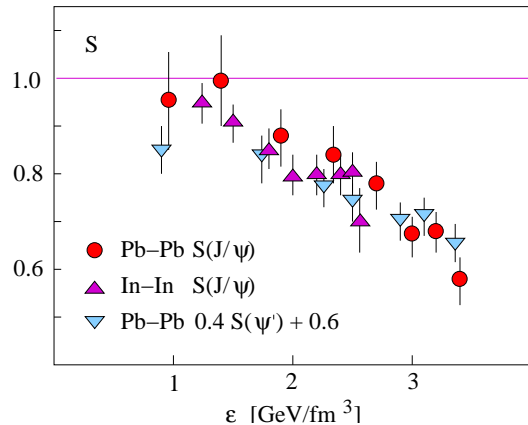


Figure 45: Universal J/ψ and ψ' suppression [76]

If the interpretation in terms of sequential suppression is correct, the data for ψ' suppression can be used to form $0.4 S_{\psi'} + 0.6$, and this should then coincide with the measured J/ψ data [76]. We show in Fig. 45 the SPS J/ψ data from $Pb-Pb$ and $In-In$ collisions together with the mentioned ψ' form. Within the present errors, this universal scaling relation seems to hold quite well. Note that here the centrality of the J/ψ data is determined by E_{ZDC} , that for the ψ' by E_T . It is obviously very important to obtain also the corresponding ψ' data with E_{ZDC} as the centrality variable.

The sequential suppression pattern expected from statistical QCD means that in most of the RHIC data as well as in the central SPS data, what is seen should be the surviving directly produced $J/\psi(1S)$. This also has consequences on the transverse momentum behaviour, which thus provide a way to check the conclusion [76]. The main effect leading

to a broadening of transverse momentum spectra in nuclear interactions is the collision broadening of the incident gluons which fuse to make $c\bar{c}$ pairs. A standard random walk analysis gives for the squared transverse momentum of the produced J/ψ [77]

$$\langle p_T^2 \rangle_{pA} = \langle p_T^2 \rangle_{pp} + N_c^A \delta_0 \quad (54)$$

in $p-A$ and to

$$\langle p_T^2 \rangle_{AA} = \langle p_T^2 \rangle_{pp} + N_c^{AA} \delta_0 \quad (55)$$

in $A-A$ collisions. Here N_c^A denotes the average number of collisions of a projectile nucleon in the target nucleus A , and N_c^{AA} the sum of the average number of collisions of a projectile nucleon in the target and vice versa, at the given centrality. The parameter δ_0 specifies the average “kick” which the incident parton receives in each subsequent collision. The crucial parameters are thus the elementary $\langle p_T^2 \rangle_{pp}$ from $p-p$ interactions and the value of δ_0 , determined by corresponding $p-A$ data; both depend on the collision energy. The behaviour of N_c^{AA} as function of centrality can be obtained through a Glauber analysis and provides the “normal” centrality dependence of $\langle p_T^2 \rangle_{AA}$.

If RHIC as well as central SPS data basically show the surviving direct J/ψ , then one should observe the p_T behaviour as given by eqs. (54) and (55). This again leads to a scaling relation for the different data sets from SPS [72] and RHIC [74]. From the RHIC $\mu^+\mu^-$ data, we obtain $\langle p_T^2 \rangle_{pp} = 2.51 \pm 0.21 \text{ GeV}^2$ and $\langle p_T^2 \rangle_{dAu} = 3.96 \pm 0.28 \text{ GeV}^2$; for the latter value, we have taken the average of the positive and negative rapidity ranges. The average number of collisions per nucleon is here found to be $N_c^A = 7.6 \pm 0.03$, so that

$$\delta_0^{RHIC} \simeq 0.19 \text{ GeV}^2 \quad (56)$$

for the parton broadening at RHIC as shown in the large rapidity data. We note here that each kinematic data set requires a separate analysis, which for the muon arm data appears possible. The central e^+e^- data so far give (with large errors) a $\langle p_T^2 \rangle$ which for $p-p$ is larger than that for $p-A$, so that here more statistics are needed. – At SPS energy, we have $\langle p_T^2 \rangle_{pp} = 1.25 \pm 0.05 \text{ GeV}^2$ and $\langle p_T^2 \rangle_{pU} = 1.49 \pm 0.05 \text{ GeV}^2$. With the same number of collisions per nucleon given by the RHIC value³ we get

$$\delta_0^{SPS} \simeq 0.033 \text{ GeV}^2 \quad (57)$$

for the corresponding parton broadening. With all parameters thus determined, we obtain as a characteristic of the transverse momentum broadening the average number of collisions of a projectile and a target nucleon in an AA collisions at the given centrality,

$$\langle N_c^{AA} \rangle = \{ \langle p_T^2 \rangle_{AA} - \langle p_T^2 \rangle_{pp} \} / \delta_0. \quad (58)$$

If our interpretation of sequential suppression is correct and the observed $\langle p_T^2 \rangle$ due to the unaffected direct J/ψ 's, then the SPS and the RHIC muon data should fall on a universal curve. We see in Fig. 46 that this is in fact the case. Once the corresponding broadening pattern for the RHIC electron data is determined, it should also follow this curve. – The normal centrality dependence of $\langle N_c^{AA} \rangle$ has also been calculated in a Glauber analysis [77]; the result is included in Fig. 46.

We thus find that the overall view of the charmonium data today is more than before in

³This should be checked separately, using the new pA data at SPS energy.

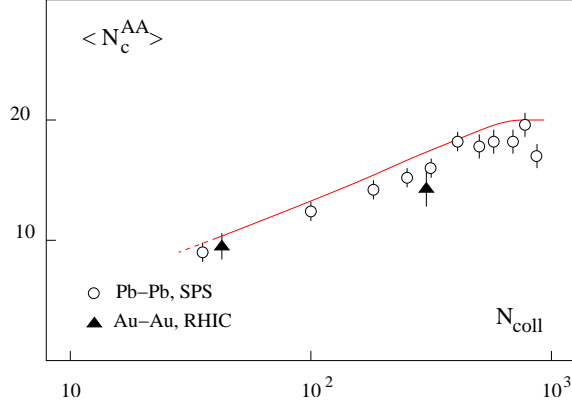


Figure 46: Transverse momentum broadening at SPS and RHIC [76]

accord with the results from statistical QCD. The crucial elements for this are

- the common onset of anomalous suppression for J/ψ and ψ' at the dissociation value $\epsilon \simeq 1 \text{ GeV}/\text{fm}^3$ expected for higher excited charmonium states; and
- the apparent suppression saturation at about 50 – 70%, following the initial onset, suggesting a survival of directly produced J/ψ 's up to much higher energy densities.

The first observation revises prior experimental indications for distinct onsets for ψ' and J/ψ suppression, at $\epsilon \simeq 1 \text{ GeV}/\text{fm}^3$ and $2.5 \text{ GeV}/\text{fm}^3$, respectively. The second observation becomes meaningful because of the revision of the theoretical claim of a direct J/ψ suppression just slightly above T_c .

It seems clear what is further needed to make these indications conclusive.

- More precise ψ' data at SPS energy (and with E_{ZDC} determined centrality) could substantiate the scaling behaviour of Fig. 45.
- More precise J/ψ data in the “saturation” regime $\epsilon \geq 3 \text{ GeV}/\text{fm}^3$ could substantiate the direct (1S) survival rate ($\sim 60\%$).
- An eventual further suppression onset at much higher ϵ (LHC?) could confirm the sequential suppression pattern predicted by statistical QCD.
- Finally, corresponding studies of the bottomonium spectrum with its different suppression onsets could provide decisive substantiation.

Given the present state of the data, any conclusions must necessarily remain tentative or even speculative. How could the picture just presented be experimentally falsified, and what would be a possible alternative account? The most frequently considered alternative is based on the possibility of J/ψ formation by “recombination”, i.e., by the binding of c and \bar{c} quarks originating from different nucleon-nucleon collisions. This approach [62] assumes two distinct mechanisms affecting J/ψ production in nuclear collisions [78]:

- A charmonium state produced in a given nucleon-nucleon interaction can be dissociated either by comover collisions or by screening effects in the hot medium. This leads to the decreasing survival probability which was labelled “thermal dissociation” in Fig. 34.

- Any two c and \bar{c} in the resulting medium, whatever their origin, can then at hadronization combine to form a charmonium state. An estimate of this recombination possibility leads in Fig. 34 to the curve labelled “statistical recombination”.
- Since the charm production rate as a hard process grows faster than the rate for light quarks, the recombination probability will increase with centrality as well as with collision energy. This will eventually lead in $A-A$ collisions to J/ψ production rates, relative to overall charm production, which are larger than those in $p-p$ collisions.

At present RHIC energy and centralities, the decreasing rate for “direct” production (i.e., in a given nucleon-nucleon collision), due to thermal dissociation, is taken to be just compensated by the increasing rate of charmonia formed by combination of charm quarks from different nucleon-nucleon collisions, thus leading to an approximately constant “saturation” regime, as seen in Figs. 40 or 44.

We should here note two specific aspects inherent in this approach. The assumed form for the decreasing thermal dissociation pattern is, as far as we know today (see section 4.) not that obtained for a QGP in statistical QCD, with its survival of $J/\psi(1S)$ up to much higher temperatures; instead, it is a phenomenological extrapolation of SPS data. As mentioned, it is not at all obvious that nuclear collisions do lead to the equilibrated QGP studied in lattice QCD, and it is also not obvious that even in such a medium, collision effects on a short-time scale could not modify the purely thermal behaviour found there (see the remarks at the end of sections 4.3 and 4.4). Nevertheless, the form used at present in the recombination approach [78] has no direct quantitative QCD basis. – Secondly, we had seen that the survival probability appears to converge to roughly the fraction (60%) of the remaining directly produced J/ψ 's. This certainly needs to be checked in more detail, but, if it were true, it would need to find some explanation in a recombination approach.

The ultimate tests to falsify one or the other approach seem in any case quite clear. The most characteristic feature of the recombination approach is an eventual *increase* of the survival probability with centrality. If observed, this would rule out a direct relation between the experimental pattern and that obtained in statistical QCD. On the other hand, if higher centralities lead to *further suppression*, and if moreover a similar pattern is found for bottomonium production, this would seem to rule out recombination of exogamous pairs as significant charmonium formation process. It thus appears that the LHC, with its higher energy density access, will still play a decisive role in obtaining the final answer to the use of quarkonium spectra as probes of the strongly interacting matter produced in nuclear collisions.

7. Outlook

The theoretical analysis of the in-medium behaviour of quarkonia has greatly advanced in the past decade. Potential model studies based on lattice results for the colour-singlet free energy as well as direct lattice calculations appear to be converging, and within a few more years, the dissociation temperatures for the different quarkonium states will be calculated precisely. Through corresponding calculations of the QCD equation of state,

these temperatures provide the energy density values at which the dissociation occurs. In statistical QCD, quarkonia thus allow a spectral analysis of the quark-gluon plasma.

The application of this analysis in high energy nuclear collisions is so far less conclusive. There exists a wealth of data from different interactions at the SPS, and first RHIC results are now also available. These results indicate the production of a hot, dense, strongly interacting medium. It is not yet clear, however, to what extent this medium is indeed the quark-gluon plasma studied in statistical QCD. Is it possible to identify dissociation onsets for different charmonium states? Does the initial (non-thermal) overabundance of charm survive a subsequent thermalization? Is the apparent J/ψ suppression saturation from SPS up to fairly central RHIC collisions the survival of the directly produced J/ψ 's as seen in lattice QCD studies, or is it the production of additional J/ψ 's through exogamous $c\bar{c}$ pairings?

It is undoubtedly very challenging to construct models incorporating as many of the observed features as possible. Nevertheless it seems worthwhile to note that measurements of the relative dissociation points of the different quarkonium states might be our only chance to compare quantitative *ab initio* QCD predictions directly to data.

Acknowledgements

In the preparation of this report, I have received stimulation and support from more colleagues than I can possibly list; but I am certainly very grateful to all of them. Particular thanks go to R. Arnaldi, S. Digal, F. Karsch, D. Kharzeev, C. Lourenço, M. Nardi and R. Vogt, whose help was really essential.

References

- [1] J. J. Aubert et al., Phys. Rev. Lett. 33 (1974) 1404;
J. E. Augustin et al., Phys. Rev. Lett. 33 (1974) 1406.
- [2] S. W. Herb et al., Phys. Rev. Lett. 39 (1977) 252.
- [3] T. Matsui and H. Satz, Phys. Lett. B 178 (1986) 416.
- [4] F. Karsch, E. Laermann and A. Peikert, Phys. Lett. B 478 (2000) 447.
- [5] F. Karsch, Lect. Notes Phys. 583 (2002) 209.
- [6] A. Peikert, F. Karsch and E. Laermann, Nucl. Phys. B 83-84 (2000) 390.
- [7] J. Engels et al., Z. Phys. C 42 (1989) 341.
- [8] M. Asakawa and T. Hatsuda, Nucl. Phys. A 610 (1996) 470c.
- [9] E. Shuryak and I. Zahed, Phys. Rev. C 70 (2004) 021901.
- [10] V. Koch, A. Majumder and J. Randrup, Phys. Rev. Lett. 95 (2005) 182301;
S. Ejiri, F. Karsch and K. Redlich, hep-ph/0509051;
R. V. Gavai and S. Gupta, hep-lat/0510044.

- [11] L. D. McLerran and B. Svetitsky, Phys. Lett. 98 B (1981) 195 and Phys. Rev. D 24 (1981) 450;
J. Kuti, J. Polónyi and K. Szlachányi, Phys. Lett. 98B (1981) 199.
- [12] F. Karsch and E. Laermann, Phys. Rev. D 50 (1994) 6954.
- [13] P. Petreczky, hep-lat/0506012.
- [14] S. Katz, Quark Matter 2005, Budapest
- [15] Z. Fodor and S. Katz, JHEP 0203 (2002) 014;
P. de Forcrand and O. Philipsen, Nucl. Phys. B 642 (2002) 290;
M.-P. Lombardo, Phys. Rev. D 67 (2003) 014505;
C. R. Allton et al., Phys. Rev. D 68 (2003) 014507.
- [16] M. A. Halasz et al., Phys. Rev. D 58 (1998) 096007.
- [17] E. Eichten et al., Phys. Rev. D 17 (1978) 3090; Phys. Rev. D 21 (1980) 203.
- [18] S. Jacobs, M. G. Olsson and C. Suchyta, Phys. Rev. 33 (1986) 3338.
- [19] S. Digal, F. Karsch and H. Satz, in preparation
- [20] M. E. Peskin, Nucl. Phys. B 156 (1979) 365;
G. Bhanot and M. E. Peskin, Nucl. Phys. B 156 (1979) 391.
- [21] D. Kharzeev and H. Satz, Phys. Lett. B 334 (1994) 155
- [22] See e.g., S. Matinyan and B. Müller, Phys. Rev. C 58 (1998) 2994;
L. Maiani et al., Nucl. Phys. A 741 (2004) 273.
- [23] D. Kharzeev and H. Satz, Phys. Lett. B 356 (1995) 365.
- [24] H. Miyazawa, Phys. Rev. D 20 (1979) 2953;
V. Goloviznin and H. Satz, Yad. Fiz. 60N3 (1997) 523
- [25] O. Kaczmarek et al., Prog. Theor. Phys. Suppl. 153 (2004) 287;
O. Kaczmarek and F. Zantow, hep-lat/0503017.
- [26] F. Karsch, M.-T. Mehr and H. Satz, Z. Phys. C 37 (1988) 617
- [27] V. V. Dixit, Mod. Phys. Lett. A5 (1990) 227.
- [28] S. Digal et al., Eur. Phys. J. C 43 (2005) 71.
- [29] S. Digal, P. Petreczky and H. Satz, Phys. Lett. B 514 (2001) 57.
- [30] L. D. Landau and E. M. Lifshitz, *Statistical Physics*, Pergamon Press, London, 1958.
- [31] O. Kaczmarek and F. Zantow, Eur. Phys. J. C 43 (2005) 63.
- [32] C.-Y. Wong, hep-ph/0408020

- [33] W. Alberico et al., hep-ph/0507084;
C.-Y. Wong, hep-ph/0509088.
- [34] D. Kharzeev, L. D. McLerran and H. Satz, Phys. Lett. B 356 (1995) 349.
- [35] T. Umeda et al., Int. J. Mod. Phys. A16 (2001) 2215;
M. Asakawa and T. Hatsuda, Phys. Rev. Lett. 92 (2004);
S. Datta et al., Phys. Rev. D 69 (2004) 094507;
H. Iida et al., hep-lat/0509129
- [36] R. Morrin et al., hep-lat/0509115.
- [37] N. Armesto et al., Phys. Rev. Lett. 77 (1996) 3736;
M. Nardi and H. Satz, Phys. Lett. B 442 (1998) 14;
H. Satz, Nucl. Phys. A 661 (1999) 104c.
- [38] L. McLerran and R. Venugopalan, Phys. Rev. D 49 (1994) 2233 and 3352; D 50 (1994) 2225;
for a recent review, see L. McLerran, Nucl. Phys. A 702 (2002) 49.
- [39] J.D. Bjorken, Phys. Rev. D27 (1983) 140.
- [40] A. D. Martin, R. G. Roberts and W. J. Stirling, Int. Journal of Mod. Phys. A 10 (1995) 2885.
- [41] M. B. Einhorn and S. D. Ellis, Phys. Rev. D12 (1975) 2007;
H. Fritzsch, Phys. Lett. 67B (1977) 217;
M. Glück, J. F. Owens and E. Reya, Phys. Rev. D17 (1978) 2324;
J. Babcock, D. Sivers and S. Wolfram, Phys. Rev. D18 (1978) 162.
- [42] H. Satz and X.-N. Wang (Eds.), *Hard Processes in Hadronic Interactions*, Int. J. Mod. Phys. A 10 (1995) 2881;
M. Mangano et al. (Eds.), *Hard Probes in Heavy-Ion Collisions at the LHC*, CERN Yellow Report 2004-09, Geneva 2004.
- [43] R. Hagedorn, Nuovo Cim. Suppl. 3 (1965) 147;
Nuovo Cim. 56A (1968) 1027.
- [44] F. Becattini, Z. Phys. C 69 (1996) 485;
F. Becattini and U. Heinz, Z. Phys. C 76 (1997) 269.
- [45] P. L. McGaughey et al., Int. J. Mod. Phys. A 10 (1995) 2999.
- [46] L. Antoniazzi et al., Phys. Rev. D 46 (1992) 4828, and Phys. Rev. Lett. 70 (1993) 383.
- [47] G. T. Bodwin, E. Braaten and G. P. Lepage, Phys. Rev. D 51 (1995) 1125;
E. Braaten and S. Fleming, Phys. Rev. Lett. 74 (1995) 3327.

- [48] T. Affolder et al. (CDF), hep-ex/0004027;
E. Braaten et al., hep-ph/9911436.
- [49] D. Kharzeev and H. Satz, Phys. Lett. B 366 (1996) 316.
- [50] Y. Lemoigne et al., Phys. Lett. 113B (1982) 509;
L. Antoniazzi et al., Phys. Rev. D 46 (1992) 4828; Phys. Rev. Lett. 70 (1993) 383;
HERA B.
- [51] F. Abe et al. (CDF), Phys. Rev. Lett. 75 (1995) 4358;
T. Affolder et al. (CDF), Phys. Rev. Lett. 84 (2000) 2094.
- [52] M. J. Leitch, Eur. Phys. J. C 43 (2005) 157.
- [53] R. Vogt, Phys. Rev. C 61 (2000) 035203.
- [54] D. Kharzeev and H. Satz, Z. Phys. C60 (1993) 389.
- [55] D. Kharzeev et al., Z. Phys. C47 (1997) 307.
- [56] B. Alessandro et al. (NA50), Eur. Phys. J. C 33 (2004) 31.
- [57] S. S. Adler et al. (PHENIX), nucl-ex/0507032
- [58] D. Kharzeev, E. Levin and M. Nardi, Nucl. Phys. A 730 (2004) 448.
- [59] R. Vogt, Phys. Rev. C71 (2005) 054902.
- [60] D. Kharzeev and M. Nardi, Phys. Lett. B 507 (2001) 121.
- [61] S. J. Brodsky and A. H. Mueller, Phys. Lett. 206 B (1988) 685;
N. Armesto and A. Capella, Phys. Lett. B 430 (1998) 23.
- [62] P. Braun-Munzinger and J. Stachel, Nucl. Phys. A690 (2001) 119;
R. L. Thews et al., Phys. Rev. C 63 (2001) 054905.
- [63] For a recent survey, see C. Pajares, Eur. Phys. J. C 43 (2005) 9.
- [64] F. Becattini et al., hep-ph/0508188
- [65] S. Gupta and H. Satz, Phys. Lett. B 283 (1992) 439.
- [66] S. Digal, P. Petreczky and H. Satz, Phys. Rev. D 64 (2001) 094015.
- [67] For a recent survey, see R. L. Thews, Eur. Phys. J. C 43 (2005) 97.
- [68] S. Digal, S. Fortunato and H. Satz, Eur. Phys. J. C 32 (2004) 547.
- [69] For recent summaries and earlier literature, see
B. Alessandro et al. (NA50), Eur. Phys. J. C 39 (2005) 335;
L. Kluberg, Eur. Phys. J. C 43 (2005) 145;
G. Borges et al. (NA50), hep-ex/0505065.

- [70] R. Arnaldi (NA60), Quark Matter 2005, Budapest
- [71] M. Sitta et al. (NA50), hep-ex/0405056.
- [72] B. Alessandro et al. (NA50) Nucl. Phys. A 721 (2003) 253;
Nucl. Phys. A 749 (2005) 243.
- [73] H. Pereira da Costa (PHENIX), Quark Matter 2005, Budapest
- [74] T. Gunji (PHENIX), PANIC2005, Santa Fe
- [75] S. S. Adler et al. (PHENIX), nucl-ex/0409015.
- [76] D. Kharzeev, F. Karsch and H. Satz, in preparation.
- [77] D. Kharzeev, M. Nardi and H. Satz, Phys. Lett. B 405 (1997) 14;
for similar earlier work, see
S. Gavin and M. Gyulassy, Phys. Lett. B 214 (1988) 241;
J. Hüfner, Y. Kurihara and H. J. Pirner, Phys. Lett. B 215 (1988) 218.
- [78] L. Grandchamp and R. Rapp, Nucl. Phys. A 709 (2002) 415.